

Quantum algorithm for dephasing of coupled systems: decoupling and IQP duality

Sabrina Yue Wang^{1,*} and Raul A. Santos^{1,†}

¹*Phasecraft Ltd.*

(Dated: 13th January 2026)

Noise and decoherence are ubiquitous in the dynamics of quantum systems coupled to an external environment. In the regime where environmental correlations decay rapidly, the evolution of a subsystem is well described by a Lindbladian quantum master equation.

In this work, we introduce a quantum algorithm for simulating unital Lindbladian dynamics by sampling unitary quantum channels without extra ancillas. Using ancillary qubits we show that this algorithm allows approximating general Lindbladians as well. For interacting dephasing Lindbladians coupling two subsystems, we develop a decoupling scheme that reduces the circuit complexity of the simulation. This is achieved by sampling from a time-correlated probability distribution—determined by the evolution of one subsystem, which specifies the stochastic circuit implemented on the complementary subsystem.

We demonstrate our approach by studying a model of bosons coupled to fermions via dephasing, which naturally arises from anharmonic effects in an electron–phonon system coupled to a bath. Our method enables tracing out the bosonic degrees of freedom, reducing part of the dynamics to sampling an **instantaneous quantum polynomial (IQP)** circuit. The sampled bitstrings then define a corresponding fermionic problem, which in the non-interacting case can be solved efficiently classically. We comment on the computational complexity of this class of dissipative problems, using the known fact that sampling from IQP circuits is believed to be difficult classically.

I. INTRODUCTION

Historically, much effort has been devoted to develop efficient quantum algorithms for unitary evolution, culminating in optimal approaches [1–7] as a function of the evolution time. This should come as no surprise as a natural application of quantum computers is to study the time evolution of quantum systems [8, 9], providing a clear path towards quantum advantage as the system size increases [10–13].

On the other hand, the study of the equally relevant time evolution of open systems, i.e. systems that evolve in the presence of external (an often uncontrolled) degrees of freedom, has received less attention [14]. In the limit of fast relaxation of the external system (often denoted as *the bath*) the time evolution of a subsystem is captured by a Lindblad master equation [15–17] that determines the dynamics of the system and can in principle realise universal quantum computation [18]. In this *Markovian* regime several quantum algorithms have been proposed to simulate open quantum dynamics [19–31] with different requirements and assumptions.

As quantum computers have yet to reach maturity, simpler albeit not optimal quantum algorithms usually perform better in practice [32–34] as their prefactors are usually smaller than the ones of theoretical optimal proposals. Mirroring this, it is natural to look for algorithms that lower the quantum resources of simulating open quantum dynamics in concrete scenarios. Motivated by this quest, here we introduce and analyse a quantum simulation algorithm that approximates the time evolution of an open quantum system generated by a *unital* Lindbladian

$$\mathcal{L}(\rho) = -i[H, \rho] + \sum_{i=1}^N \left(L_i \rho L_i - \frac{1}{2} \{L_i^2, \rho\} \right), \quad (1)$$

where L_i is an hermitian but otherwise arbitrary operator. A unital Lindbladian \mathcal{L} is a Lindbladian that has the identity operator as a fixed point i.e $\mathcal{L}(\mathbb{I}) = 0$ and is the generator of a *unital quantum channel* $\mathcal{E}_t := e^{t\mathcal{L}}$ that preserves the identity operator as $\mathcal{E}(\mathbb{I}) = \mathbb{I}$. We achieve this by approximating this unital quantum channel by a *mixed unitary channel* $\mathcal{E}(\rho) := \sum_k p_k U_k \rho U_k^\dagger$, where $0 \leq p_k \leq 1$ and $\sum_k p_k = 1$ i.e \mathcal{E} is a convex combination of unitary channels [35]. Due to their structure, mixed unitary channels can be interpreted as the expected channel obtained by applying a stochastic unitary channel sampled from a probability distribution p_k . This generates an efficient way of approximating them.

Unital Lindbladians cannot decrease the entropy, and their dissipative part tends to destroy quantum coherence. As the identity operator is a fixed point of the evolution, one may ask about the classical complexity of simulating

* sabrina@phasecraft.io

† raul@phasecraft.io

them. After all, if the quantum coherences are being erased and the system is driven to the infinite temperature state, is a quantum computer even needed to simulate these systems? While this intuition is correct if the Lindbladian evolution has a unique steady state and the evolution time is sufficiently long, the dynamics is actually nontrivial in the presence of symmetries, or if the Lindbladian has other fixed points. For example, in the physics of fermions hopping on a lattice and subject to dephasing [36] it has been shown that the Lindbladian, although unital, is gapless in the thermodynamic limit, leading to nontrivial long time behaviour. Moreover, several open problems about the interplay of dephasing and coherent dynamics exist, ranging from its role in the many body localisation transition [37–42], its effect in quantum transport [37, 43–45], the breaking of topological order [46], to the effect of dephasing in the quantum-classical transition [47].

Here we argue for the general computational hardness of this approach from a different perspective. We study bipartite systems where the jump operator $L_i = A_i B_i$ acts nontrivially in subsystems \mathcal{S}_A and \mathcal{S}_B . For this scenario we develop a decoupling scheme that allows one to trace out one of the subsystems. This result is highlighted in [Theorem 2](#), and used to study the problem of electron-phonon coupling due to anharmonicity in [Section III B](#). There we show explicitly that after tracing out the phonon degrees of freedom, the evolution in the fermionic sector is determined by sampling an IQP circuit, something that is expected to be difficult classically [48, 49]. The decoupling scheme presented in [Theorem 3](#) also allows the efficient systematic study of *non-Markovian* dissipation on a quantum computer, something that to our knowledge has not been discussed extensively.

A. Relation to previous work

Several algorithms for the quantum simulation of Lindbladian dynamics has been developed. In [19] the first algorithm for simulating Lindbladians by Trotterisation was discussed, leading to a $O(t^2/\epsilon)$ scaling of gate complexity with evolution time t and error ϵ (omitting factors related with the system size). In [20] the authors improve on this to $O(t^{3/2}/\sqrt{\epsilon})$. Assuming sparse quantum jump operators represented by an oracle, they also provide an algorithm with query complexity $O((t^2/\epsilon)\text{polylog}(t/\epsilon))$. This result was improved in [21] where a performance of $O(t \text{polylog}(t/\epsilon))$ is achieved using linear combination of unitaries. A quantum algorithm achieving this same scaling but without compressed encoding has been discussed in [25]. In [22, 23] an unravelling approach to the simulation of Lindbladian dynamics is presented, where non-unitary operators are approximated by sums of unitaries, although without a complexity analysis. The same technique of splitting a generic operator into two unitaries but using the quantum singular value transform is discussed in [26]. Refs. [30] and [31] provide different algorithms for embedding the non-unitary dynamics into a Hamiltonian evolution, the former using a numerical scheme to map the unravelled equation into a dilated Hamiltonian problem while the latter uses repeated interactions and measurement. An approach to estimate the matrix elements needed to compute the Lindblad equation is presented in [24]. On the classical side, novel algorithms based on unravelling the evolution equation [50] and sampling trajectories in a tensor network framework has been introduced in [51].

Motivated by the constraints of current quantum capabilities, cheaper practical algorithms for simulation have also been explored. In [27] a variational quantum algorithm has been proposed. It uses a parameterised circuit to time evolve a vectorised representation of the density matrix. In [28] the authors show that any Lindblad dynamics can be simulated using one bath qubit, with repeated resets. In the same context of simplifying quantum algorithms, [29] combines second-order Trotter formulas with randomisation to approximate Lindbladian evolution via sampling from a distribution over unitaries.

Our contribution

In this work we explore sampling unitaries that implement unital channels, much in the same spirit as in [29], where no ancilla qubits are needed, but where the type of non-unitary evolutions are constrained to mixed unitary channels. We depart from [29] in two respects:

- We concentrate on the generator [Eq. \(1\)](#) and provide an explicit mixed-unitary channel that approximates it. The gate complexity for an approximation of the evolution up to time t and precision ϵ scales as to $O(t^2/\epsilon)$
- We introduce the decoupling [Theorem 3](#) that allows the study of coupled systems (as in [Theorem 2](#)) by reducing the evolution of the coupled system to two different Hamiltonian simulation problems where the bitstring output of one determines the circuit in the other and the expectation of this process generates the full dynamics.

We exemplify this algorithm by studying a model of electrons coupled to phonons. Tracing the bosonic degrees of freedom corresponding to the phonons, we find that the evolution in the fermionic subsystem is determined by a

mixed unitary channel with a *time dependent* probability distribution that corresponds to the measurement outcomes of an IQP circuit. This non-Markovian evolution of the fermions is further investigated by sampling (in emulation) the IQP circuit over 10 qubits, allowing us to fully simulate the system classically over 10 trotter steps.

The paper is organised as follows, in [Section II](#) we motivate and present the main results. In [Section III](#) we discuss some applications of the main results in concrete settings. In [Section III A](#) we highlight the connection with disordered systems while in [Section III B](#) we use these results to study the effect of electron-phonon coupling on a physical system. By exactly tracing out the bosonic degrees of freedom, we obtain an effective description of the system in terms of a mixed unitary channel on the fermionic sector, with probabilities associated with an IQP circuit with a number of qubits proportional to the number of Trotter steps. We study the properties of the emergent IQP circuit and discuss the full quantum algorithm in this context. We show the result of the time evolution of the electron-phonon system in [Section IV](#), where we observe the effect of the dissipation on the fermionic system induced by the coupling through dephasing with the bosonic bath. Finally in [Section V](#) we discuss some broader implications of our work in terms of the hardness of classical simulation of unital Lindbladian evolution.

II. MAIN RESULTS

A. Motivation

Let's consider the unital Lindbladian with Hamiltonian H and quantum jump operator $L = L^\dagger$

$$\mathcal{L}(\rho) = -i[H, \rho] + L\rho L - \frac{1}{2}\{L^2, \rho\}, \quad (2)$$

where the first term captures the coherent evolution of the system while the second describes dephasing induced by the environment. The dissipative evolution $e^{t\mathcal{L}}$ generated by [Eq. \(2\)](#) can be approximated by

$$\mathcal{E}(\rho) := e^{-iHt} \frac{1}{2} (e^{i\sqrt{t}L} \rho e^{-i\sqrt{t}L} + e^{-i\sqrt{t}L} \rho e^{i\sqrt{t}L}) e^{iHt} = e^{t\mathcal{L}}(\rho) + O(t^2), \quad (3)$$

as all the odd powers in \sqrt{t} cancel. This expression can be interpreted as the expectation of an stochastic channel $\mathcal{U}_s(\rho) := e^{-iHt} e^{s_i \sqrt{t}L} \rho e^{-s_i \sqrt{t}L} e^{iHt}$, where the random variable $s = \{+, -\}$ is sampled uniformly. From this result the following theorem follows

Theorem 1 (Dissipative Dynamics - simplified). *The time evolution with the unital Lindblad operator*

$$\mathcal{L}(\rho) = -i[H, \rho] + \sum_{i=1}^{N_L} \left(L_i \rho L_i - \frac{1}{2}\{L_i^2, \rho\} \right), \quad (4)$$

where N_L is the number of jump operators in the dissipative component and L_i is hermitian, can be approximated by the expectation value of the stochastic channel

$$\mathcal{U}_s(\rho) := e^{-iHt} \left(\prod_{j=1}^{N_L} e^{s_j i \sqrt{t} L_j} \rho e^{-s_j i \sqrt{t} L_j} \right) e^{iHt}, \quad (5)$$

where each $s_j = \pm 1$ in $s = (s_1, \dots, s_{N_L})$ is a uniformly distributed random variable with probability distribution $p_s = \frac{1}{2^{N_L}}$. The error incurred in this approximation is

$$\left\| \mathbb{E}(\mathcal{U}_s(\rho)) - e^{t\mathcal{L}}(\rho) \right\|_\diamond = \left\| \sum_{s=\{+,-\}^{N_L}} p_s \mathcal{U}_s(\rho) - e^{t\mathcal{L}}(\rho) \right\|_\diamond = O(t^2), \quad (6)$$

for $t \in [0, 1]$.

We prove this theorem in [Section A](#). Unital Lindbladians are defined as convex combinations of unitary channels so this connection is not extremely surprising. In the case of interacting unital Lindbladians, where the jump operator acts nontrivially in two subsystems, we can extend this result as follows. Consider now a bipartite system $\mathcal{S} = \mathcal{S}_A \cup \mathcal{S}_B$ and the dephasing Lindbladian

$$\mathcal{L}(\rho) = AB\rho AB - \frac{1}{2}\{(AB)^2, \rho\}, \quad (7)$$

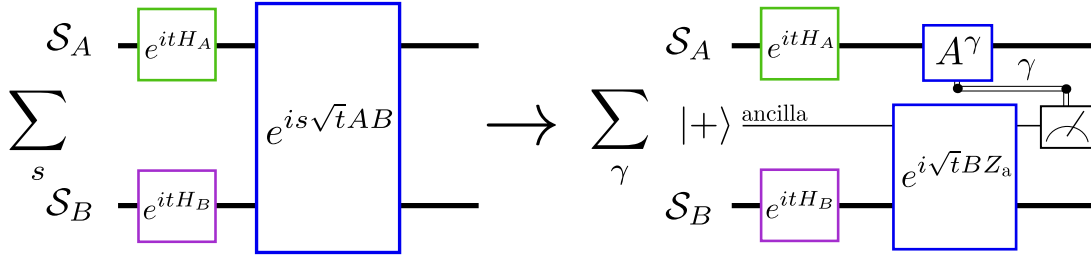


Figure 1. Decoupling gadget: The average of a channel with interaction term $e^{is\sqrt{t}AB}$ where $s = \{-1, 1\}$ can be expressed as the outcome of a different channel where one subsystem is coupled to an ancilla through the Pauli Z operator and then the ancilla is measured. The result of that measurement defines the circuit that is implemented in the other subsystem.

where $A \in \mathcal{S}_A$ and $B \in \mathcal{S}_B$ are hermitian operators satisfying $[A, B] = 0$ and $A^2 = 1$. For simplicity we do not consider any coherent evolution for now as it can be easily added back. This Lindbladian generates the evolution $e^{t\mathcal{L}}(\rho)$ and can as before, be approximated by the convex combination of unitary channels

$$\mathcal{E}(\rho) := \frac{1}{2}(e^{i\sqrt{t}BA}\rho e^{-i\sqrt{t}BA} + e^{-i\sqrt{t}BA}\rho e^{i\sqrt{t}BA}) = e^{t\mathcal{L}}(\rho) + O(t^2) \quad (8)$$

Using that $A^2 = 1$ we can decompose the channel \mathcal{E} into the sum

$$\mathcal{E}(\rho) = \sum_{\gamma=0,1} \frac{A^\gamma}{2} \sum_{s^+, s^- = \pm} e^{i\sqrt{t}Bs^+} \rho e^{-i\sqrt{t}Bs^-} (s^+ s^-)^\gamma \frac{A^\gamma}{2}. \quad (9)$$

This form motivates defining the state $|+\rangle = \frac{1}{\sqrt{2}}(|1\rangle + | - 1\rangle)$ which is the $+1$ eigenstate of the Pauli X operator, such that

$$\mathcal{E}(\rho) = \sum_{\gamma} A^\gamma \langle \gamma | e^{i\sqrt{t}BZ} | + \rangle \rho \langle + | e^{-i\sqrt{t}BZ} | \gamma \rangle A^\gamma, \quad (10)$$

where $|\gamma\rangle := Z^\gamma |+\rangle$ is the eigenstate of X with eigenvalue $(-1)^\gamma$. This decomposition is very suggestive as it completely decouples the product of operators A and B at the cost of coupling B with an extra spin (qubit) degree of freedom (see Fig. 1).

Taking the partial trace with respect to the subsystem \mathcal{S}_B on a separable density matrix $\rho = \rho_{\mathcal{S}_A} \otimes \rho_{\mathcal{S}_B}$ we have

$$\text{Tr}_{\mathcal{S}_B}(\mathcal{E}(\rho_{\mathcal{S}_A} \otimes \rho_{\mathcal{S}_B})) = \sum_{\gamma} p_{\gamma} A^\gamma \rho_{\mathcal{S}_A} A^\gamma, \quad (11)$$

where p_{γ} corresponds to the probability of measuring the state $|\gamma\rangle$ on the ancilla after evolving the initial decoupled density matrix between the ancilla and the system, i.e.

$$p_{\gamma} := \text{Tr}(e^{i\sqrt{t}BZ} \rho_{\text{aux}} \otimes \rho_{\mathcal{S}_B} e^{-i\sqrt{t}BZ} |\gamma\rangle \langle \gamma|) \quad (12)$$

where $\rho_{\text{aux}} = |+\rangle \langle +|$. What have we gained with this? From Eq. (11), we see that to simulate the original dissipative evolution, we can first simulate the system \mathcal{S}_B coupled to the ancillary qubit and based on the outcome of measuring the ancillary qubit in the γ basis perform a unitary evolution in \mathcal{S}_A . This decoupling mechanism is always beneficial when the coupling appears just in the dissipative term compared with the direct simulation of the entire system as the ancillary system does not have its own dynamics. Adding back the the unitary evolution and several types of couplings we find the result

Theorem 2 (Dissipative Decoupled Dynamics: Dcube). *Given a system $\mathcal{S} = \mathcal{S}_A \cup \mathcal{S}_B$, a Hamiltonian $H = H_A + H_B$ where $H_{A/B}$ acts only in its respective subspace, and hermitian jump operators $L_i = A_i B_i$ with $[A_i, B_j] = 0$ and $A_j^2 = 1 \forall j$, where $A_i (B_i)$ acts nontrivially on $\mathcal{S}_A (\mathcal{S}_B)$, the time evolution generated by the unital Lindbladian*

$$\mathcal{L}(\rho) = -i[H, \rho] + \sum_{i=1}^{N_L} \left(L_i \rho L_i - \frac{1}{2} \{L_i^2, \rho\} \right), \quad (13)$$

over a time t can be approximated by introducing an ancillary qubit system \mathcal{S}_C such that

$$e^{t\mathcal{L}}(\rho) = \sum_{\gamma=\{0,1\}^{N_L}} U_{\gamma}^{(A)} \text{Tr}_C(V^{(B,C)} \rho \otimes \rho_C V^{\dagger(B,C)} \Pi_{\gamma}) U_{\gamma}^{\dagger(A)} + O(t^2) \quad (14)$$

with $U_{\gamma}^{(A)} := e^{-itH_A} \prod_{j=1}^{N_L} A_j^{\gamma_j}$, $V^{(B,C)} := e^{-itH_B} \prod_{j=1}^{N_L} e^{i\sqrt{t}B_j Z_j}$, $\rho_C = \otimes_{i=1}^{N_L} |+\rangle\langle+|_i$ and Π_{γ} is a projector onto the state $|\gamma\rangle := |\gamma_1, \dots, \gamma_{N_L}\rangle$ where $|\gamma\rangle$ is the eigenstate of the Pauli X matrix with eigenvalue $(-1)^{\gamma}$.

The usefulness of this result is highlighted in the following lemma

Lemma 3 (Decoupling lemma). *Assuming the same conditions as in Theorem 2; the time evolution of an initially unentangled density matrix between the subsystems $\rho_0 = \rho_A \otimes \rho_B$ on the system \mathcal{S}_A can be approximated as*

$$\rho_A(t) = \text{Tr}_{\mathcal{S}_B}(e^{t\mathcal{L}}(\rho_0)) = \sum_{\gamma=\{0,1\}^{N_L R}} \text{Tr}(V_t(\rho_B \otimes \Pi_0) V_t^{\dagger} \Pi_{\gamma}) U_{\gamma,t}(\rho_A) U_{\gamma,t}^{\dagger} + O(t^2/R) \quad (15)$$

where $U_{\gamma,t} := \prod_{k=1}^R \left(e^{-i\frac{t}{R}H_A} \prod_{j=1}^{N_L} A_j^{\gamma_{jk}} \right)$ and $V_t := \prod_{j=1}^R \left(e^{-i\frac{t}{R}H_B} \prod_{k=1}^{N_L} e^{i\sqrt{\frac{t}{R}}B_k Z_{j,k}} \right)$. Here Π_{γ} is a projector onto the state $|\gamma\rangle := \otimes_{j,k} |\gamma_{j,k}\rangle$ where $|\gamma\rangle$ is the eigenstate of the Pauli X matrix with eigenvalue $(-1)^{\gamma}$. Z denotes the conventional Pauli matrix.

This means that to simulate the time evolution on \mathcal{S}_A we can stochastically sample unitary evolutions defined only on \mathcal{S}_A according to a probability distribution that is governed by the evolution of \mathcal{S}_B coupled to a number of qubits that grow with the number of Trotter steps.

The different algorithms for **time dynamics simulation (TDS)** of open systems in the context of Theorem 1 and Theorem 2 are presented below as pseudocode in Algorithms 1 and 2. In the next section we discuss applications of these algorithms, in particular the connection with the study of disordered systems Section III A and the physics of electron-phonon coupled systems Section III B.

B. Extension to general Lindbladians

Up to this point, we have concentrated in the approximation of unital Lindbladians, which, by virtue of Theorem 1 are implementable sampling unitary channels. Using ancillas, it is possible to generalise this arbitrary Lindbladians. Consider the map Eq. (3) with the hermitian Lindblad operator $L = (\ell\sigma_a^+ + \ell^{\dagger}\sigma_a^-)$.

$$\mathcal{E}(\rho) := e^{-iHt} \frac{1}{2} \left(e^{i\sqrt{t}(\ell\sigma_a^+ + \ell^{\dagger}\sigma_a^-)} \rho e^{-i\sqrt{t}(\ell\sigma_a^+ + \ell^{\dagger}\sigma_a^-)} + e^{-i\sqrt{t}(\ell\sigma_a^+ + \ell^{\dagger}\sigma_a^-)} \rho e^{i\sqrt{t}(\ell\sigma_a^+ + \ell^{\dagger}\sigma_a^-)} \right) e^{iHt}, \quad (16)$$

here ℓ is some arbitrary operator on the target system ρ_s and $\sigma_a^{\pm} = \frac{1}{2}(X_a \pm iY_a)$ is the common raising/lowering operator acting on an ancillary qubit. Applying this map to the density matrix $\rho = \rho_s \otimes (|0\rangle\langle 0|)_a$ using Theorem 1 and tracing away the ancillary qubit generates the approximation

$$\text{Tr}_a(\mathcal{E}(\rho_s(|0\rangle\langle 0|)_a)) = e^{t\mathcal{L}}(\rho_s) + O(t^2) \quad (17)$$

with

$$\mathcal{L}(\rho_s) = -i[H, \rho_s] + \ell\rho_s\ell^{\dagger} - \frac{1}{2}\{\ell^{\dagger}\ell, \rho_s\}. \quad (18)$$

Adding more ancillas this can be trivially generalised to the case of different jump operators.

III. APPLICATIONS

A. Connection with simulation of disordered systems

Theorem 1 can be used to show that dephasing appears naturally in the study of disordered systems, where the value of an observable corresponds to the ensemble average over some disorder distribution. Here we show explicitly that for particular disordered systems, the average over disorder corresponds to a Lindbladian evolution with dephasing and rescaled parameters.

Algorithm 1: Approximating the time evolution of systems with dephasing

Result: An approximation of the expectation of a time evolved operator $\hat{O}(t)$ under the Lindbladian

$$\mathcal{L}(\rho) = -i[H, \rho] + \sum_{j=1}^N L_j \rho L_j - \frac{1}{2} \{L_j^2, \rho\}$$

Given a Hamiltonian $H = \sum_{k=1}^l h_k$ and a set of quantum jump operator L_j with $j \in \{1, \dots, N_L\}$ where h_k and L_j are operators such that e^{ith_k} and $e^{i\sqrt{t}L_j}$ are directly implementable, a state ρ_0 , an operator \hat{O} , an evolution time t a number of Trotter steps R and a number of measurements M ,

for $p = 1..M$ **do**

- Sample the $N_L \times R$ random variables $\mathbf{s} := \{\{s_{jk}\}_{j=1}^{N_L}\}_{k=1}^R$ from the uniform distribution where $s_{jk} = \{-1, 1\}$.
- Construct the unitary

$$U_{\mathbf{s}} := \prod_{r=1}^R \left(\prod_{k=1}^l e^{-i\frac{t}{R}h_k} \prod_{j=1}^{N_L} e^{s_{j,r}i\sqrt{\frac{t}{R}}L_j} \right)$$

- Measure $x_p := \text{Tr}(U_{\mathbf{s}}\rho_0 U_{\mathbf{s}}^\dagger \hat{O})$

end

Output $\frac{1}{M} \sum_{p=1}^M x_p$

Algorithm 2: Approximating the time evolution of systems interacting through dephasing

Result: An approximation of the expectation of a time evolved operator $\hat{O}(t)$ under Lindbladian evolution

$$\mathcal{L}(\rho) = -i[H, \rho] + \sum_{j=1}^{N_L} A_j B_j \rho B_j A_j - \frac{1}{2} \{B_j^2, \rho\} \text{ with } A_j^2 = 1 \text{ and } [B_j, A_k] = 0 \forall j, k$$

Given a Hamiltonian $H = H_A + H_B$ with H_α acting on subsystem \mathcal{S}_α and $H_\alpha = \sum_{k=1}^l h_{\alpha,k}$ and a set of quantum jump operator $A_j B_j$ with $j \in \{1, \dots, N_L\}$ where $h_{\alpha,k}$ and B_j are operators such that $e^{ith_{\alpha,k}}$ and $e^{i\sqrt{t}B_j Z_a}$ are directly implementable, with Z_a a Pauli Z operator acting on an ancilla qubit; a state ρ_0 , an operator \hat{O} , an evolution time t a number of Trotter steps R and a number of measurements M

for $p = 1..M$ **do**

- Construct the state $\rho_C := \otimes_{i=1}^{N_L R} |+\rangle\langle +|_i$ using $N_L R$ ancillas
- Define the unitary

$$V := \prod_{j=1}^R \left(\prod_{k=1}^l e^{-i\frac{t}{R}h_{B,k}} \prod_{k=1}^{N_L} e^{i\sqrt{\frac{t}{R}}B_k Z_{j,k}} \right)$$

and the circuit $V\rho_0 \otimes \rho_C V^\dagger$

- Measure the ancillas in the X Pauli basis. Store the resulting bitstring as γ_p .
The remaining state is $\tilde{\rho}$
- Define the unitary $U_\gamma := \prod_{k=1}^R \left(\prod_{k=1}^l e^{-i\frac{t}{R}h_{A,k}} \prod_{j=1}^{N_L} A_j^{\gamma_{jk}} \right)$ and the circuit $U_\gamma \tilde{\rho} U_\gamma^\dagger$.
- Measure $x_p := \text{Tr}(U_\gamma \rho_0 U_\gamma^\dagger \hat{O})$

end

Output $\frac{1}{M} \sum_{p=1}^M x_p$

More precisely, consider the task of simulating the evolution under a random Hamiltonian $H(\xi) := H_0 + \xi H_1$, where ξ is sampled according to some probability distribution $p(\xi)$ and the results are averaged over $p(\xi)$. Consider the following disorder average of a time evolved operator O on the state $|\Psi\rangle$

$$\mathbb{E}\langle O(t) \rangle_\xi := \mathbb{E}(\langle \Psi | e^{itH(\xi)} O e^{-itH(\xi)} | \Psi \rangle) := \sum_{\xi} p(\xi) \langle \Psi | e^{itH(\xi)} O e^{-itH(\xi)} | \Psi \rangle \quad (19)$$

where we assume that $\xi \in [a, b]$ is sampled uniformly. Here $H_{0,1}$ are Hamiltonians that are independent of the random variable ξ . We can rescale ξ in terms of a new random variable $\tilde{\xi}$ uniformly distributed in the interval $[0,1]$ as $\tilde{\xi} := \frac{\xi-a}{b-a}$.

Using the binary representation of ξ we have

$$\tilde{\xi} = \sum_{n=1}^{\infty} \frac{\xi_n}{2^n} \rightarrow \xi = (b - a) \sum_{n=1}^{\infty} \frac{\xi_n}{2^n} + a \quad (20)$$

where $\xi_n \in \{0, 1\}$ is a discrete random variable. Finally, defining $s_n := 2\xi_n - 1 \in \{-1, 1\}$ we have

$$H(\xi) = H_0 + \xi H_1 = H_0 + \frac{(b+a)H_1}{2} + \sum_{n=1}^{\infty} s_n \frac{(b-a)}{2^{n+1}} H_1 \quad (21)$$

The first order Trotterisation of the evolution by this Hamiltonian is

$$e^{itH(\xi)} = e^{it(H_0 + \frac{a+b}{2}H_1)} \prod_{n=1}^{\infty} e^{s_n i \sqrt{t} (\sqrt{t}(b-a) \frac{H_1}{2^{n+1}})} + O(t^2) \quad (22)$$

Using [Theorem 1](#) we find that the average channel $\mathbb{E}(U_{\xi} \rho U_{\xi}^{\dagger}) = \sum_{\xi} p(\xi) e^{itH(\xi)} \rho e^{-itH(\xi)}$ is approximated by the Lindbladian

$$\mathcal{L}(\rho) = -i[H_0 + \frac{a+b}{2}H_1, \rho] + \frac{t(b-a)^2}{12} \left(H_1 \rho H_1 - \frac{1}{2} \{H_1^2, \rho\} \right) \quad (23)$$

with an error $O(t^2)$ as long as $b - a \sim O(t^{-\frac{1}{2}})$. This implies that the disorder average with a disorder sampled from an interval that decreases like $t^{-\frac{1}{2}}$ can be approximated by a Lindbladian evolution where the dephasing is induced by the disordered term. For other disorders, the dephasing process is not captured by a time independent and local Lindbladian, but can still be captured by a mixed unital quantum channel, of which a generator in time can be defined.

B. Electron-phonon systems

The main application of [Theorem 2](#) that we consider in this work is the dynamics of electrons coupled to phonons, where the coupling appears in the form of a quantum jump operator $\ell_i = n_i x_i$ composed of the electron density n_i and the position operator of the boson around the lattice site i , x_i . This quantum jump operator induces coupled dissipative dynamics on an electronic system representing electrons on a lattice and a bosonic system representing phonon modes related to the vibrations of the lattice around its equilibrium position. As it is common, we consider only one phononic mode per lattice site, corresponding to the coupling with the most relevant optical phonon mode. These type of interactions have been considered in the context of pure Hamiltonian description in the Holstein [\[52\]](#) and Fröhlich Hamiltonians [\[53, 54\]](#). The former includes localised electron-phonon coupling and is able to capture the emergence of polaron quasiparticles (particles where the charge is dressed by lattice distortions, creating a net (multi)pole). In contrast the latter includes long-range interactions and serves to understand symmetry breaking phenomena like BCS-superconductivity [\[55\]](#) and the formation of charge-density waves [\[56\]](#). These models often work in the harmonic approximation, where the purely bosonic Hamiltonian is reduced to an harmonic potential. Moreover, in this context the **electron-phonon coupling (EPC)** terms are also often limited to a single electron coupled to a single phonon.

There is a rich history of methods developed to study electron-phonon models, from Feynman's variational path-integral formalism [\[57\]](#) to **diagrammatic Monte Carlo (DMC)** [\[58–60\]](#). Feynman's approach is a semi-analytical theory, where all bosonic degrees of freedom are traced away and their effects incorporated in fermionic self-interactions. This theory has been shown to fail in dynamical scenarios [\[61\]](#) and intermediate coupling regimes [\[62\]](#). To address dynamics, **DMC** performs a Wick rotation to map the problem into imaginary time, avoiding large oscillations in real time evolution. As a result analytical continuation is needed to recover back the real time signal. This procedure is in practice ill-defined and without theoretical guarantees of convergence. Recent works have attempted to circumvent this issue by using symbolic analytical continuation [\[63, 64\]](#), which better controls the rotation back to real time, but also lack guarantees in general.

The accurate treatment of anharmonic effects is computationally challenging [\[65, & references therein\]](#) but essential for understanding real materials. For example, in a material approaching a structural phase transition some vibration modes will have a frequency going to zero in the harmonic case. Including non-harmonic contributions controls the type of structural transition that occurs [\[66\]](#). Similarly, phonon-phonon interactions, a direct consequence of anharmonicity, greatly alter electron-phonon scattering rates in the study of transport [\[67\]](#).

Recently, several proposals to study these anharmonic effects have appeared in the literature, by extending analytic methods [65], self-consistently through **self-consistent phonon (SCP)** theory [68–70], or using coupled cluster [71] and **quantum Monte Carlo (QMC)** [72].

In this section we study anharmonic effects in the dynamical evolution of an electron-phonon system by analysing a system composed of subsystems F which is fermionic, Q and B bosonic, each with internal dynamics described by the Hamiltonians H_F , H_Q and H_B respectively. We assume the following anharmonic coupling

$$H_c = \frac{1}{2} \sum_{i=1}^L g_i (q_i^\dagger + q_i)(b_i^\dagger + b_i)(f_i^\dagger f_i - \frac{1}{2}), \quad (24)$$

where q_i (q_i^\dagger) is the bosonic destruction (creation) operator corresponding to a Brownian particle at site i , b_i^\dagger and b_i are bosonic creation and destruction operators of an external bath, and f_i (f_i^\dagger) are fermionic destruction (creation) operators, all defined at the same lattice site. Assuming an harmonic bath, it is possible to trace the effect of the bath by expanding the von Neumann equation to second order in the anharmonic interaction. This procedure (see [Section B](#) for details), generates the following Lindbladian

$$\mathcal{L}(\rho) = -i[H_F + H_Q, \rho] + \frac{1}{4} \sum_{j=1}^L g_j^2 \mathcal{L}_{x_j(2n_j-1)}(\rho), \quad (25)$$

$$= -i[H_F + H_Q, \rho] + \sum_{j=1}^L g_j^2 \left(x_j \mathcal{L}_{n_j}(\rho) x_j + \frac{1}{4} \mathcal{L}_{x_j}(\rho) \right), \quad (26)$$

with $\mathcal{L}_\ell(\rho) := \ell \rho(t) \ell^\dagger - \frac{1}{2} \{ \ell^\dagger \ell, \rho \}$ and $x_j = \frac{q_j + q_j^\dagger}{\sqrt{2}}$. Here the usual dephasing Lindbladian for electrons $\mathcal{L}_{n_j}(\rho)$ [73] is multiplied by the position of the quantum Brownian particle, producing an interaction dependent dephasing on the fermionic sector. $\mathcal{L}_x(\rho)$ is the dissipative term appearing in **quantum Brownian motion (QBM)** [74], a prevalent model describing systems coupled to bosonic baths. Traditional methods to tackle the **QBM** part using **Born-Markov master equation (BMME)** [16, 75–77] often violates the positivity condition of the density matrix due to the loss of Markovianity in the construction, and lead to the break-down of Heisenberg's uncertainty principle. Using a Lindbladian construction [78] these problems dissapear.

The Lindbladian [Eq. \(25\)](#) satisfies the requirements of the decoupling [Theorem 3](#) and as such the electron-phonon dynamics can be completely decoupled via the introduction of Ising-like variables (ancillary qubits) that mediate interactions between the subsystems F and Q . This is very useful as it allows completely tracing the bosonic degrees of freedom. This result is captured in the following lemma

Lemma 4. (*Boson - Qubit duality in dissipative evolution.*) *The fermionic density matrix $\rho_F(t) = \text{Tr}_Q(e^{t\mathcal{L}}\rho(0))$ of a system evolving under the Lindbladian [Eq. \(25\)](#)*

$$\mathcal{L}(\rho) = -i[H_F + H_Q, \rho] + \frac{1}{4} \sum_{j=1}^L g_j^2 \mathcal{L}_{x_j(2n_j-1)}(\rho), \quad (27)$$

where $H_Q = \sum_{j=1}^L \omega_j q_j^\dagger q_j$ is a sum of harmonic Hamiltonians over all the bosons and the initial state is unentangled $\rho(0) = \rho_F \otimes |0\rangle\langle 0|$, can be approximated to arbitrary accuracy by the mixed unital channel

$$\rho_F(t) = \sum_{\gamma=\{0,1\}^{LN}} \text{Tr} \left(e^{t\mathcal{L}_{\text{IQP}}(t)} (\Pi_0) \Pi_\gamma \right) U_{\gamma,t}(\rho_F) U_{\gamma,t}^\dagger + O(t^2/N), \quad (28)$$

following the definitions of [Theorem 3](#) and the effective Lindbladian on the ancilla qubits

$$\mathcal{L}_{\text{IQP}}(t)[\rho] := -i[H_{\text{IQP}}(t), \rho] + \sum_{k=1}^L \left(\ell_k(t) \rho \ell_k^\dagger(t) - \frac{1}{2} \{ \ell_k^\dagger(t) \ell_k(t), \rho \} \right), \quad (29)$$

where $H_{\text{IQP}}(t) := \sum_{k=1}^L \frac{g_k^2}{8N} \sum_{j>l} Z_{j,k} Z_{l,k} \sin \left(\omega_k \frac{(l-j)t}{N} \right)$, $\ell_k(t) = \frac{g_k}{2} \sqrt{\frac{1}{2N}} \sum_{j=1}^N e^{i\omega_k \frac{jt}{N}} Z_{j,k}$ and N is the number of Trotter steps.

Proof. Directly applying [Theorem 3](#) on the Lindbladian Eq. (25), we have

$$\rho_F(t) = \sum_{\gamma=\{0,1\}^{LN}} \text{Tr} \left(V_t(\rho_Q \otimes \Pi_0) V_t^\dagger \Pi_\gamma \right) U_{\gamma,t}(\rho_F) U_{\gamma,t}^\dagger + O(t^2/N), \quad (30)$$

where

$$V_t := \prod_{j=1}^N \left(e^{-i\frac{t}{N}H_Q} \prod_{k=1}^L e^{i\sqrt{\frac{t}{N}}g_k \frac{x_k}{2} Z_{j,k}} \right) = e^{-itH_Q} \prod_{j=1}^N \left(\prod_{k=1}^L \exp \left[\frac{ig_k}{2} \sqrt{\frac{t}{N}} x_k \left(\frac{jt}{N} \right) Z_{j,k} \right] \right). \quad (31)$$

The last equality is an identity that follows from the repeated application of

$$e^{-tA} e^{-tB} e^{-tA} e^{-tB} = e^{-2tA} (e^{tA} e^{-tB} e^{-tA}) (e^{-tB}) = e^{-2tA} (e^{-tB(t)}) (e^{-tB(0)}), \quad (32)$$

and $x_j(t) := e^{itH_Q} x_j e^{-iH_Q t}$. Assuming a quadratic Hamiltonian for the quantum Brownian particle $H_Q := \sum_i \omega_i q_i^\dagger q_i$, the time evolved operator $x_j(t)$ becomes simply $x_j(t) = \frac{1}{\sqrt{2}}(q_j e^{-i\omega_j t} + q_j^\dagger e^{i\omega_j t})$. In this case we can combine all the products in V_t Eq. (31) over a single site using the Baker-Campbell-Haussdorff (BCH) relation $e^A e^B = e^{A+B} e^{\frac{1}{2}[A,B]}$, valid whenever $[A, B]$ commutes with A and B . After some straighforward algebra we find

$$V_t = e^{-itH_Q} \prod_{k=1}^L \exp \left(\frac{ig_k}{2} \sqrt{\frac{t}{2N}} \sum_{j=1}^N \left[(q_k e^{-i\omega_k \frac{jt}{N}} + q_k^\dagger e^{i\omega_k \frac{jt}{N}}) Z_{j,k} \right] \right) e^{-\frac{ig_k^2 t}{8N} \sum_{j>l} Z_{j,k} Z_{l,k} \sin(\omega_k \frac{(l-j)t}{N})}.$$

Introducing the displacement operator $D(\alpha) := e^{\alpha^\dagger - \alpha}$, and defining $\eta_k = \left[-\frac{ig_k}{2} \sqrt{\frac{t}{2N}} \sum_{j=1}^N e^{-i\omega_k \frac{jt}{N}} Z_{j,k} \right]$ Eq. (30) becomes

$$\rho_F(t) = \sum_{\gamma=\{0,1\}^{NR}} \text{Tr} \left(e^{-itH_{\text{IQP}}(t)} D(\mathbf{q} \cdot \boldsymbol{\eta}) (\rho_Q \otimes \Pi_0) D(-\mathbf{q} \cdot \boldsymbol{\eta}) e^{itH_{\text{IQP}}(t)} \Pi_\gamma \right) U_{\gamma,t}(\rho_F) U_{\gamma,t}^\dagger + O(t^2/N) \quad (33)$$

with $\mathbf{q} \cdot \boldsymbol{\eta} = \sum_{k=1}^L q_k \eta_k$ and $H_{\text{IQP}}(t) := \sum_k \frac{g_k^2}{8N} \sum_{j>l} Z_{j,k} Z_{l,k} \sin(\omega_k \frac{(l-j)t}{N})$. Finally, assuming that the initial state of the quantum Brownian particle is the vaccum, and using the algebra of the displacement operator $D(\mathbf{q} \cdot \boldsymbol{\eta}) = e^{-\frac{1}{2}\boldsymbol{\eta}^* \cdot \boldsymbol{\eta}} e^{\mathbf{q}^\dagger \cdot \boldsymbol{\eta}^*} e^{\mathbf{q} \cdot \boldsymbol{\eta}}$ that follows from BCH, we have

$$\text{Tr}_Q (D(\mathbf{q} \cdot \boldsymbol{\eta}) (\rho_Q \otimes \Pi_0) D(-\mathbf{q} \cdot \boldsymbol{\eta})) = e^{-\frac{1}{2}\boldsymbol{\eta}^* \cdot \boldsymbol{\eta}} \text{Tr}_Q \left(e^{\mathbf{q}^\dagger \cdot \boldsymbol{\eta}^*} |0\rangle \langle 0| \Pi_0 \langle 0| e^{\mathbf{q} \cdot \boldsymbol{\eta}} \right) e^{-\frac{1}{2}\boldsymbol{\eta}^* \cdot \boldsymbol{\eta}}. \quad (34)$$

It is possible to compute the trace over the boson degrees of freedom by writing the projector Π_0 in the computational basis of the ancillary Ising qubits. In this basis the exponents on each side of the projector act as phases in the ancillary space. Concretely

$$\text{Tr}_Q \left(e^{\mathbf{q}^\dagger \cdot \boldsymbol{\eta}^*} |0\rangle \langle 0| e^{\mathbf{q} \cdot \boldsymbol{\eta}} \right) = \frac{1}{2^{LN}} \sum_{\mathbf{s}, \mathbf{s}'} |\mathbf{s}\rangle \langle \mathbf{s}'| \langle 0| e^{\mathbf{q} \cdot \boldsymbol{\eta}(\mathbf{s}')} e^{\mathbf{q}^\dagger \cdot \boldsymbol{\eta}^*(\mathbf{s})} |0\rangle = \frac{1}{2^{LN}} \sum_{\mathbf{s}, \mathbf{s}'} |\mathbf{s}\rangle \langle \mathbf{s}'| e^{\boldsymbol{\eta}^*(\mathbf{s}) \cdot \boldsymbol{\eta}(\mathbf{s}')} \quad (35)$$

where we have used the BHC relation $e^A e^B = e^{[A,B]} e^B e^A$ and that the vacuum is invariant under the action of the exponential of bosonic destruction operators. Putting everything together we have

$$\rho_F(t) = \sum_{\gamma=\{0,1\}^{LN}} \text{Tr} \left(e^{t\mathcal{L}_{\text{IQP}}(t)} (\Pi_0) \Pi_\gamma \right) U_{\gamma,t}(\rho_F) U_{\gamma,t}^\dagger + O(t^2/N) \quad (36)$$

where

$$\mathcal{L}_{\text{IQP}}(t)[\rho] := -i[H_{\text{IQP}}(t), \rho] + \sum_{k=1}^L \left(\ell_k(t) \rho \ell_k^\dagger(t) - \frac{1}{2} \left\{ \ell_k^\dagger(t) \ell_k(t), \rho \right\} \right), \quad (37)$$

and $\ell_k(t) = \frac{g_k}{2} \sqrt{\frac{1}{2N}} \sum_{j=1}^N e^{i\omega_k \frac{jt}{N}} Z_{j,k}$. □

This is a remarkable result. It implies that the (dissipative) evolution of a fermion-boson system Eq. (25) can be approximated to arbitrary precision with a fermion-qubit (dissipative) evolution. The evolution on the fermion-qubit side can be understood as the result of sampling the probability distribution of the ancillary qubits

$$\Gamma_{\gamma}(t) := \text{Tr} \left(e^{t\mathcal{L}_{\text{IQP}}(t)} (\Pi_0) \Pi_{\gamma} \right), \quad (38)$$

and according to the outcome γ applying the unitary $U_{\gamma,t}$ on the fermionic system. Classically sampling from this type of probability distributions, which fall under the category of IQP circuits, even approximately is $\#P$ -hard [49]. Finding an efficient classical protocol to do so would collapse the polynomial hierarchy at the third level [48]. Of course, this does not prevent the classical simulation of this *particular* family of circuits, but nonetheless we think this connection is particularly interesting, hinting to the classical complexity of the problem and giving IQP circuits a concrete application in quantum simulation.

In the next section we discuss a circuit construction to approximate the Linbladian on the ancilla qubits, thus providing a concrete realisation of Theorem 4.

C. Circuit construction of auxiliary dissipative Lindbladian

Using Theorem 4, we can approximate the density matrix of the fermionic system by sampling the bitstring γ from the probability $\Gamma_{\gamma}(t)$. This corresponds to sampling from an IQP circuit, where all the gates are commuting. The generator of this evolution is the Linbladian Eq. (29) composed of two contributions, one given by H_{IQP} which can be trivially implemented using a circuit with no ancillas, and the dissipative part whose circuit approximation we discuss here. Writing explicitly the action of these contributions we find

$$\Gamma_{\gamma}(t) = \langle \oplus | U_{\text{IQP}}(t) e^{t\mathcal{D}_{\text{IQP}}(t)} (\Pi_0) U_{\text{IQP}}^{\dagger}(t) | \oplus \rangle \quad (39)$$

where $|\oplus\rangle = (H|0\rangle)^{\otimes NL}$ is the superposition of all computational basis states on NL qubits and H is the Hadamard gate, while

$$U_{\text{IQP}}(t) = e^{-itH_{\text{IQP}}(t)} \quad (40)$$

is the unitary part of the evolution. Note that for the IQP circuit time is a parameter that determines the circuit and not a usual time variable of a time independent Hamiltonian. The purely dissipative part is generated by

$$\mathcal{D}_{\text{IQP}}(t)[\rho] := \sum_{k=1}^L \left(\ell_k(t) \rho \ell_k^{\dagger}(t) - \frac{1}{2} \{ \ell_k^{\dagger}(t) \ell_k(t), \rho \} \right) = \sum_k \mathcal{D}_k(t)[\rho], \quad (41)$$

with the jump operators $\ell_k(t) = \frac{g_k}{2} \sqrt{\frac{1}{2N}} \sum_{j=1}^N e^{i\omega_k \frac{jt}{N}} Z_{j,k}$.

We can approximate the density matrix $\rho_k(t) := e^{t\mathcal{D}_k(t)}[\rho]$ with arbitrary small error by defining the map

$$G_{k,\epsilon}[\rho] := \text{Tr}_a (e^{\frac{i}{2}\epsilon((\ell_k + \ell_k^*)X - i(\ell_k - \ell_k^*)Y)} \rho |0\rangle \langle 0|_a e^{-\frac{i}{2}\epsilon((\ell_k + \ell_k^*)X - i(\ell_k - \ell_k^*)Y)}) \quad (42)$$

with an ancillary qubit a initialised in the $|0\rangle$ state. Here the Pauli matrices X, Y act on ancillary space of the qubit a . This map approximates \mathcal{D}_k with an error of order ϵ^4 as by taking the trace over the ancillary qubit we find

$$G_{k,\epsilon}[\rho] = \cos(\epsilon|\ell_k|) \rho \cos(\epsilon|\ell_k|) + \sin(\epsilon|\ell_k|) e^{i\ell_k/|\ell_k|} \rho \sin(\epsilon|\ell_k|) e^{-i\ell_k^*/|\ell_k|}, \quad (43)$$

$$= \rho + \epsilon^2 \left(\ell_k(t) \rho \ell_k^{\dagger}(t) - \frac{1}{2} \{ \ell_k^{\dagger}(t) \ell_k(t), \rho \} \right) + O(\epsilon^4) = e^{\epsilon^2 \mathcal{D}_k}(\rho) + O(\epsilon^4), \quad (44)$$

and the Trotterised evolution of G into N slices (with conventional error scaling as $\epsilon^2 = \frac{t}{N}$) gives

$$e^{t\mathcal{D}_k(t)}[\rho] = \left(e^{\frac{t}{N}\mathcal{D}_k(t)} \right)^N [\rho] = \left(G_{k,\sqrt{\frac{t}{N}}}[\rho] \right)^N + O\left(\frac{t^2}{N}\right). \quad (45)$$

Given the commuting property of \mathcal{D}_{IQP} it is possible to use either multiple ancillas to perform the N applications of $G_{k,\sqrt{\frac{t}{N}}}$ and trace, or use one ancilla with reset, without the need for feedforward. This has to be repeated L times as $e^{t\mathcal{D}_{\text{IQP}}(t)} = \prod_{k=1}^L e^{t\mathcal{D}_k(t)}$. In practice if the product of exponentials of Paulis are the implementable gates available,

implementing the map $G_{k,\epsilon}$ in Eq. (42) requires a further Trotterisation. Using a p -order product formula $S_p(t)$ that approximates $G_{k,\sqrt{\frac{t}{N}}}$ we have

$$G_{k,\sqrt{\frac{t}{N}}} = (G_{k,\frac{1}{N\rho}\sqrt{\frac{t}{N}}})^{N\rho} = S_p \left(\frac{1}{N\rho} \sqrt{\frac{t}{N}} \right) + O \left(\frac{1}{N\rho^p} \left(\frac{t}{N} \right)^{\frac{p+1}{2}} \right). \quad (46)$$

To retain the same overall error of the Trotterisation in Eq. (28), we can choose for example $p = 1$, $N\rho = O(N)$, $p = 2$ and $N\rho = O(N^{1/4})$ or $p = 4$ and $N\rho = O(1)$.

D. Nontrivial steady states of \mathcal{L}_{IQP}

The ancillary Lindbladian Eq. (29) has one trivial fix point corresponding to the fully mixed density matrix $\mathbb{I}/2^{LN}$ as $\mathcal{L}_{\text{IQP}}(t)[\mathbb{I}] = 0$. This motivates the question: Does the dynamics in the ancillary system tend to a trivial infinite temperature state? As the Lindbladian is diagonal in the computational basis, we can read off directly its eigenvalues. The real part of the eigenvalues controls the decay, so we concentrate on the eigenvalues of $\mathcal{D}_{\text{IQP}}(t)$. The eigenmatrices of the dissipator $\mathcal{D}_{\text{IQP}}(t)$ are $\sigma_{\mathbf{s},\mathbf{s}'} := |\mathbf{s}\rangle\langle\mathbf{s}'|$ where \mathbf{s} is a bitstring in the computational basis of the ancillas. The eigenvalues $\mathcal{D}_{\text{IQP}}(t)\sigma_{\mathbf{s},\mathbf{s}'} = \lambda_{\mathbf{s},\mathbf{s}'}\sigma_{\mathbf{s},\mathbf{s}'}$ are trivially

$$\lambda_{\mathbf{s},\mathbf{s}'} = \sum_k \left[\ell_{k,\mathbf{s}}(t)\ell_{k,\mathbf{s}'}^*(t) - \frac{1}{2} (|\ell_{k,\mathbf{s}}(t)|^2 + |\ell_{k,\mathbf{s}'}(t)|^2) \right] = -\frac{1}{2} \sum_k |\ell_{k,\mathbf{s}}(t) - \ell_{k,\mathbf{s}'}(t)|^2 + i \sum_k \Im(\ell_{k,\mathbf{s}}(t)\ell_{k,\mathbf{s}'}^*(t)), \quad (47)$$

with $\ell_{k,\mathbf{s}}(t) = \frac{g_k}{2} \sqrt{\frac{1}{2N} \sum_{j=1}^N e^{i\omega_k \frac{jt}{N}}} \mathbf{s}_{j,k}$. The real part of the eigenvalue controls the decay of the corresponding eigenmatrix. Note that for the diagonal eigenmatrices $\sigma_{\mathbf{s},\mathbf{s}}$ the real part vanishes. In order to understand the approach to a steady state, we need to see how the Lindbladian gap behaves as the number of Trotter steps increases to keep a fixed error for larger times. We can upper bound the real part of the gap by looking at the eigenmatrices $\sigma_{\mathbf{s},\mathbf{s}+\boldsymbol{\eta}}$ where the sum in the index is understood modulo 2. For these eigenmatrices, the real part of the eigenvalue is

$$|\Re(\lambda_{\mathbf{s},\mathbf{s}+\boldsymbol{\eta}})| = \frac{1}{2} \sum_k \frac{g_k}{8N} \left| \sum_{j=1}^N e^{i\omega_k \frac{jt}{N}} \boldsymbol{\eta}_{j,k} \right|^2 \leq \frac{g_{\max} L}{16N} |\boldsymbol{\eta}|^2 \quad (48)$$

where $g_{\max} = \max_k g_k$, and $|\boldsymbol{\eta}|$ is the Hamming weight of the bitstring $\boldsymbol{\eta}$. This implies that for any off diagonal element $\sigma_{\mathbf{s},\mathbf{s}+\boldsymbol{\eta}}$ with $|\boldsymbol{\eta}| = o(\sqrt{N})$ the real part of $\lambda_{\mathbf{s},\mathbf{s}+\boldsymbol{\eta}}$ vanishes in the limit $N \rightarrow \infty$. Then the long time limit of the evolution is nontrivial as the states (in the computational basis) that survive the decay live on a band of size $o(\sqrt{N})$ around the diagonal.

IV. NUMERICAL RESULTS

A. Free fermion dimer coupled to bosons

So far we have discussed theoretically a framework for approximating dephasing Lindbladian evolution. In Section III B we provide explicit error bounds and a precise protocol for the specified type of electron-phonon interaction. In this section, we numerically demonstrate the results presented in Theorem 4, which studies how to simulate the electron-phonon Lindbladian described by Eq. (25). Here we perform detailed analyses on a spinless fermionic system of two sites shown in Fig. 2, also known as the dimer. Based on this we will refer to this system as the dimer in the following discussion.

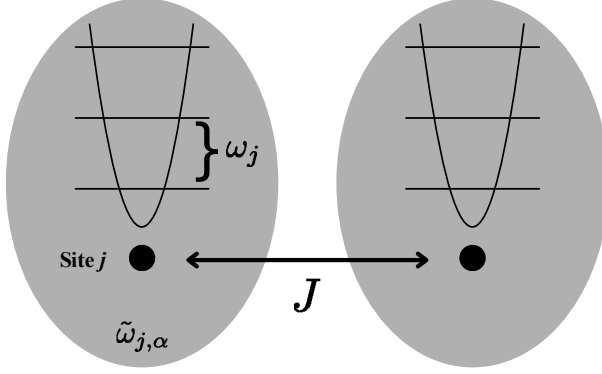


Figure 2. Schematic of the dimer in the presence of a bath and quantum Brownian particles on each site. Physical sites are denoted by the black circles with site index j . The harmonic oscillator with energy level spacing ω_j denote the Brownian particle on each site, relating to the Hamiltonian H_Q . The gray oval encompassing the entire site represents the boson bath with a continuum of energy levels $\tilde{\omega}_{j,\alpha}$ (see also Section B). On each site, the bath, Brownian particle and fermions are all coupled together with interaction strength g_j . Fermions can hop between the sites with hopping strength J and are described by the Hamiltonian H_F .

More specifically, the fermion and boson subsystem Hamiltonians from Eq. (25) under consideration are

$$H_F = \sum_{\langle i,j \rangle, \sigma} -J(c_{i,\sigma}^\dagger c_{j,\sigma} + c_{j,\sigma}^\dagger c_{i,\sigma}) + U n_{i,\uparrow} n_{i,\downarrow},$$

$$H_Q = \sum_j \omega_j q_j^\dagger q_j \quad (49)$$

where J is the fermion hopping amplitude across nearest neighbours, $n_{i,\sigma}$ the fermion number operator for site i and spin $\sigma = \uparrow$ (WLOG we restrict to the spin up sector), and ω_j the harmonic oscillator frequency for the Brownian particle on site j . For this section, we set $J = 1$, $U = 0$, $\omega_j = 1$, $g_j = g, \forall j$ and consider the system with one fermion. Wherever it is relevant, we truncate the boson Hilbert space to contain at most eight energy levels ($N_b = 8$). In general for a system on L sites with N_b boson levels per site, the number of qubits needed for the simulation scales as $L(\log_2(N_b) + 1)$. This classical simulation scales very unfavorably since the size of the matrices involved at worst grows as $2^{2L(1+\log_2(N_b))} = 2^{16}$ for this spinless case, where the additional factor of two in the exponential comes from the full density matrix simulation.

We choose to initialise the state of the Brownian particles in the vacuum and populate a single fermion on site one. The fermion density dynamics for this site, $\text{Tr}(n_1 e^{t\mathcal{L}} \rho(0))$ (where \mathcal{L} is given by Eq. (27)) is simulated with various methods and shown in Fig. 3. The solid lines named ‘exact evolution’ are the density matrix time evolutions according to Eq. (25). We will refer to this method as ‘exact Lindbladian’. It is important to note that the ‘exact Lindbladian’ evolution also suffers from error, primarily from the truncation of the infinite dimensional Hilbert space associated with the Brownian particles. We expand upon this problem in Section IV A 1. A naïve strategy to tackle this is to study convergence of observables by incrementally changing the boson Hilbert space cutoff. However this can be computationally demanding, highlighting another issue with general simulations involving bosons. Therefore, when comparing Dcube against ‘exact Lindbladian’ for general simulations involving bosons, it is imperative to account for the effect of boson truncation on the fermion observables, because Dcube implicitly takes into the account the infinite bosonic Hilbert space.

Theorem 1 allows us to directly simulate the ‘exact Lindbladian’ evolution, through the expectation over stochastic channels. This is denoted as the ‘stochastic’ method and cuts down the statevector simulation cost down to $2^{L(1+\log_2(N_b))}$. The ‘circuit’ curves correspond to the Dcube algorithm, with N Trotter steps to approximate the true Lindbladian evolution (without truncating the boson Hilbert space) by sampling from the probability distribution of the ancillary qubits, $\Gamma_\gamma(t)$ given by Eq. (39). The fermion density is then computed via a Monte Carlo estimate of the full summation

$$\text{Tr}(n_i \rho_F(t))_{\text{circuit}} = \frac{1}{N_s} \sum_x \text{tr} \left(n_i U_{\gamma_x, t}(\rho_F) U_{\gamma_x, t}^\dagger \right) \quad (50)$$

with N_s samples. The errors associated with the ‘stochastic’ and ‘circuit’ methods are computed as $\frac{\sigma}{\sqrt{N_s}}$ where σ denote the standard deviation od a particular observable computed from N_s samples. Since in our case the fermion subsystem H_F is non-interacting, Eq. (50) is computed efficiently classically via **Fermionic Linear Optics (FLO)** [79] after the circuit samples are collected. In the implementation of $\Gamma_\gamma(t)$ in Eq. (39), a second order Trotter decomposition is used to realise the map for the dissipative evolution $e^{t\mathcal{D}_{IQP}(t)}$ in Eq. (41). In order to retain an overall error of $O(\frac{1}{N})$, the number of these internal Trotter steps is set to $N_\rho = \lceil N^{\frac{1}{4}} \rceil$ and $N_\eta = N$ ancillas are used to realise Eq. (41).

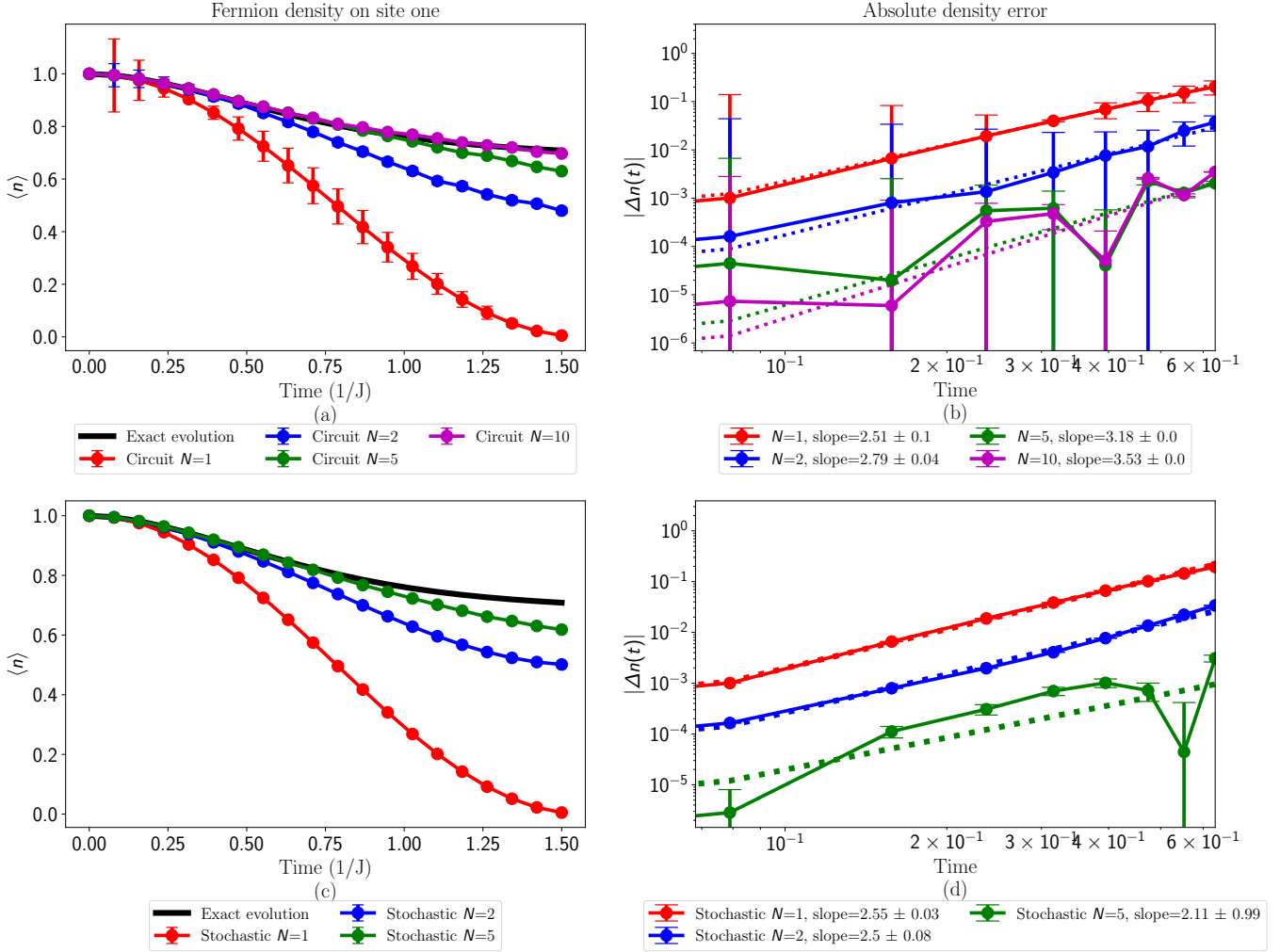


Figure 3. Density time dynamics of the spinless free fermion dimer induced by the dephasing Lindbladian of Eq. (25) compares (a) ‘exact Lindbladian’ against ‘circuit’ method with the fermion density absolute error in (b). The dashed lines are linear fits to the logarithm of the absolute density error with the slopes in the respective legend according to N Trotter steps. The number of ancillas to realise the auxiliary dissipative Lindbladian in Eq. (41) is always set equal to the total number of Trotter steps, $N_\eta = N$. Each application of this map uses $N_\rho = \lceil N^{\frac{1}{4}} \rceil$ internal Trotter steps. A total of 10k samples are taken per experiment across all different Trotter steps for the ‘circuit’ method. Similarly, the time dynamics of (c) ‘exact Lindbladian’ against ‘stochastic’ method with absolute fermion density error are compared in (d). 5k samples of uniformly sampled stochastic channels are used across all N Trotter steps. $N_b = 8$ is set for ‘exact Lindbladian’ and ‘stochastic’ simulations. The initial state is a Fock state with a single fermion on site one and $g = 4$ across all simulations.

Figure 3 also exhibits fermion number density error scaling $|\Delta n^f|$ between the ‘exact Lindbladian’ vs Trotter approximations on the right column. Visibly, the logarithmic error grows linearly in time with a slope larger than the one expected from the overall first order Trotter scaling. For reference, the expected sampling noise, $\epsilon_{\text{sampling}}$, at $N_s = 10k$ is on the order of $\epsilon_{\text{sampling}} \sim 10^{-2.4}$ which contributes to the standard deviation of the results. Furthermore, the boson truncation in the ‘exact Lindbladian’ simulations contribute to errors on a similar order of magnitude, as

examined below in Section IV A 1.

1. Dependence on Hilbert space truncation

Consider again time dynamics using the ‘exact Lindbladian’ simulation method where the boson Hilbert space is truncated. The boson number density evolution is shown on the LHS of Fig. 4. Assume there is no knowledge of the $N_b = 4$ curves. Notice that the boson number density for $N_b = 2$ on each site, shown as dashed lines in Fig. 4, never reaches the maximum allowed value of one, but appears to equilibrate well below it. Therefore, one may be inclined to set the cut-off at $N_b = 2$. However, increasing the truncation level result in the bosons following completely different dynamics and settling into a new, higher equilibrium. This reflects the fact that truncating the boson subspace *changes* the Hamiltonian for which the dynamics are simulated. This effect also manifests in the fermion dynamics where there is visible deviation between the $N_b = 2$ vs $N_b = 4$ fermion densities. The RHS of Fig. 4 shows the absolute difference in fermion density using different truncations of the bosonic Hilbert space. This variation is on the scale of 10^{-2} when comparing $N_b = 4$ and $N_b = 8$. In light of this, one should be mindful when comparing Dcube against ‘exact’ simulations such as that in Fig. 3, because the latter always involves a truncation of the bosonic Hilbert space.

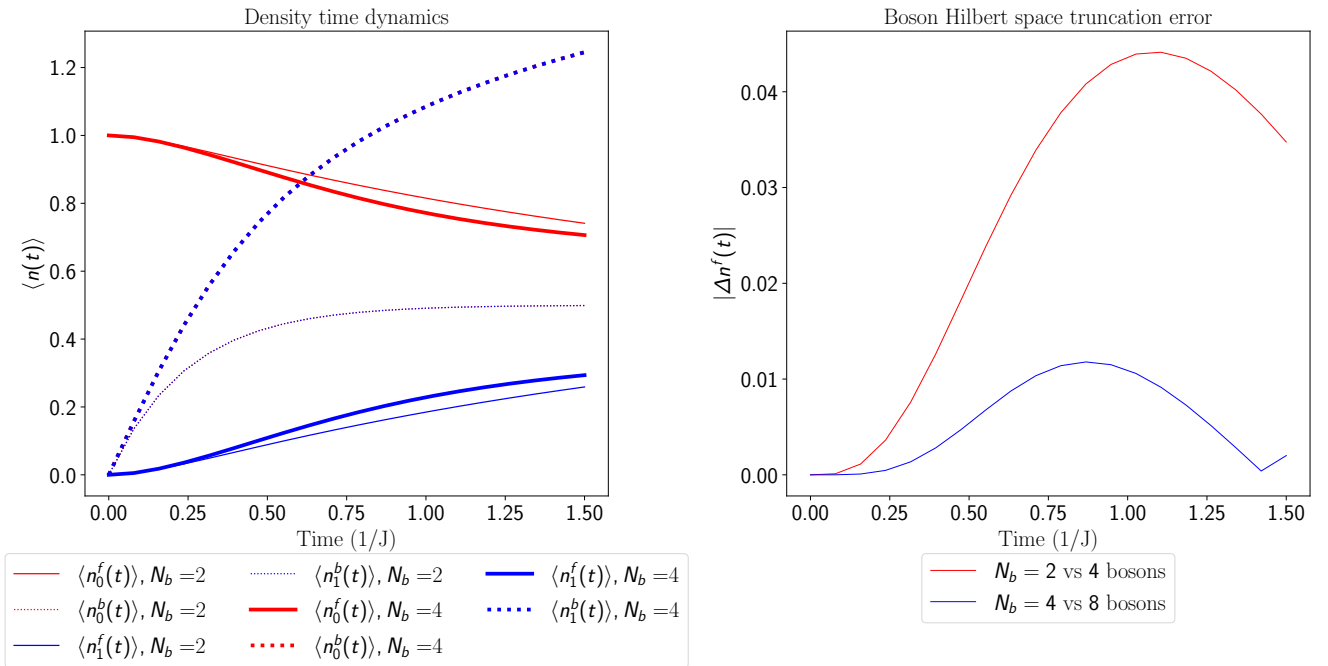


Figure 4. (LHS) Time dynamics of particle density of a spinless Fermi-Hubbard dimer under the Lindbladian Eq. (25). $\langle n_i^d \rangle$ represents the number density of site $i \in [0, 1]$ and particle identity $d \in [f, b]$ ($f = \text{fermion}$, $b = \text{boson}$), for two instances of N_b . The initial state is a single fermion on site $i = 0$. Each plot is associated with the boson truncation level of maximum $N_b - 1$ bosons per site. (RHS) The maximum change in fermion density across all sites with increasing boson Hilbert space dimension in the ‘exact Lindbladian’ simulations for the dimer at $g = 4$.

The effect of the truncation is dependent on the interaction strength. To see this, a particular limit is illuminating. Consider for example the Holstein Hamiltonian [52] in real space using the same conventions for fermions and bosons as we have throughout the rest of the text,

$$H = H_F + \frac{1}{2} \sum_i (\omega_i^2 x_i^2 + p_i^2) + \sum_i g_i x_i c_i^\dagger c_i, \quad (51)$$

where p_i is the momentum operator of the boson particle. When the fermionic occupation is full, such that $\langle n_{i,f} \rangle$ is constant and fixed for all sites i , the purely bosonic Hamiltonian can be written as

$$H - H_F = \frac{1}{2} \sum_i \left(\omega_i x_i + \frac{g_i \langle n_{i,f} \rangle}{\omega_i} \right)^2 + \frac{1}{2} p_i^2 \quad (52)$$

and is valid up to adding a constant. In this regime, it follows from Eq. (52) that the boson position operator shifts to a new equilibrium depending on g_i . Intuitively, a higher average displacement means a higher harmonic oscillator energy and hence a larger boson population. Consequently this simple limit shows that truncating the bosonic Hilbert space has to be done appropriately, carefully studying the convergence of the results as a function of truncation. For a similar analysis on the behavior of a different observable with changing the boson truncation level, see Section C following the discussion in Section IV B.

2. Behaviour of auxiliary dissipative Lindbladian Γ distribution

In this work we have uncovered a relationship between dissipative Lindbladian dynamics and IQP circuits. This suggests that although the evolution is dissipative in nature, it may be hard to capture it classically. This is because to carry out this computation it is necessary to sample from IQP circuits. In this section, we show numerically that the probability distribution arising from these circuits for small system sizes quickly become non-trivial, which we take as an indication that sufficiently long time simulations can be difficult. Theoretically, it has been shown that, assuming the polynomial hierarchy does not collapse, efficiently simulating the natural outputs of IQP can be classically hard [80–82]. In Fig. 5, we explicitly present the behaviour of the probability distribution Eq. (39) for the spinless dimer example discussed in Section IV A, for various times T with two first order Trotter step (i.e. a total of four qubits). It shows that an initially peaked distribution at $T = 0$ becomes anti-concentrated as time increases.

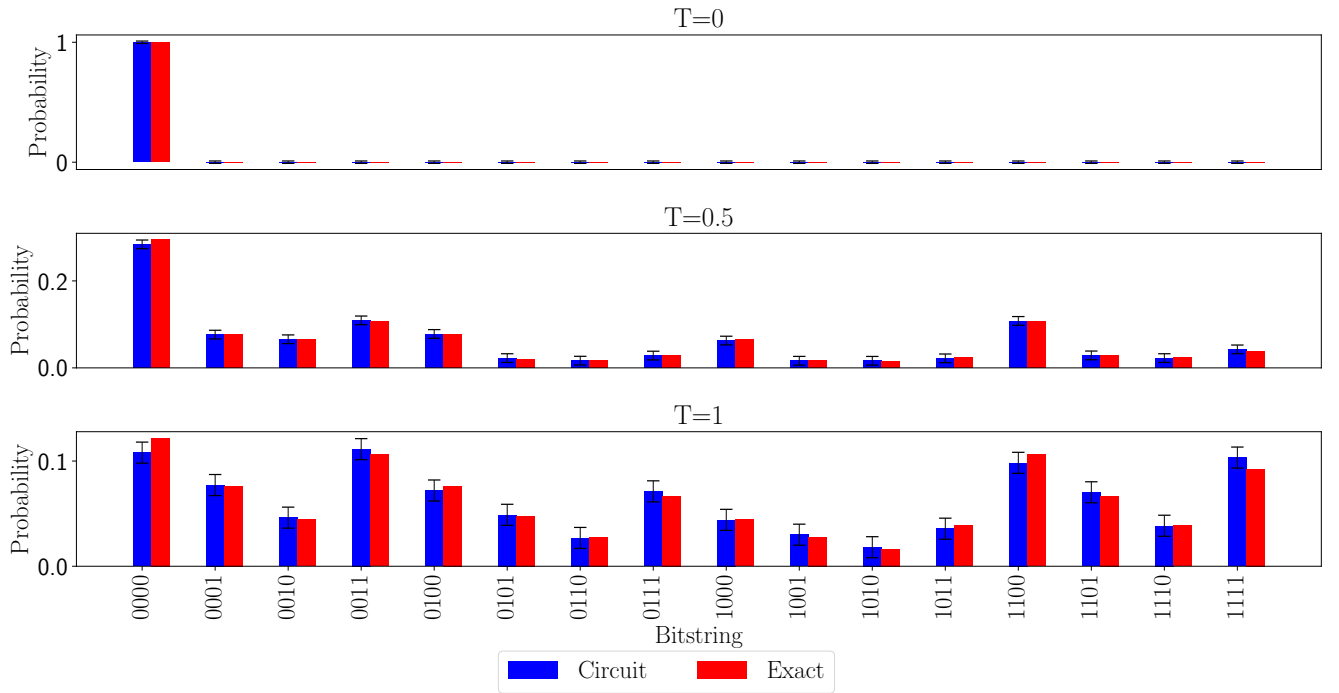


Figure 5. The full decomposition of the probability distribution of the dimer $\Gamma(t)$ for different bitstring γ s at various fixed total evolution time. $g = 4$, $\omega = J = 1$, $N_\eta = 5$ and $N_\rho = 2$ and $N = 2$ first order Trotter steps. The ‘exact’ method refer to exactly computing $\Gamma(t)$. The ‘circuit’ method refers to sampling from the corresponding noiseless IQP circuit that approximates $\Gamma(t)$. $N_s = 10k$ samples were drawn and the error bars signify the sampling error $\frac{1}{\sqrt{N_s}}$.

The ‘exact’ implementation is the exact computation of Eq. (39). The ‘circuit’ results are computed by sampling from the noiseless circuit that approximates Γ as discussed in Section III C. Note that due to site independence, rather than sampling once from a circuit of LN qubits, one can also stitch together L samples of a circuit of N qubits. At $t = 0$, Eq. (39) is simply the all-zero bitstring and the $\Gamma(0)$ is simply a delta function, melting into a different IQP distribution at each time.

B. Green's function of the spinful Fermi-Hubbard dimer under various dephasing

In this section, we show the usefulness of [Theorem 1](#) and [Theorem 2](#) in cutting down the computational cost compared to exact Lindbladian simulation. We consider the effects of two different dephasing Lindbladians on the interacting Fermi-Hubbard dimer at half-filling with zero spin along the z -direction, i.e. $S_z = 0$ (such that there is a total of one spin up and one spin down electron). Consider such a system subject to two dephasing Lindbladians. The first is the electron-phonon Lindbladian described by [Eq. \(25\)](#). The second is similar but purely fermionic in nature, given by [Eq. \(53\)](#)

$$\mathcal{L}_e(\rho) := -i[H_F, \rho] + \sum_{j=1}^L g_j^2 \mathcal{L}_{n_j}(\rho). \quad (53)$$

This type of Lindbladians describes the usual dephasing of electrons in materials and has been recently studied in refs [83, 84] in the context of dissipation induced heating dynamics. In this section, we consider the spinful dimer so the spin index in [Eq. \(49\)](#) runs over $\sigma \in [\uparrow, \downarrow]$ and $U = 0, 4, 8$ (in units of hopping J). All other system variables are kept the same as defined in [Section IV A](#). We would like to compare the actions of [Eq. \(53\)](#) and [Eq. \(25\)](#) on the **Local Density Of States (LDOS)** [85], an intrinsic quantity describing a system's electronic structure as well as information of the excitation spectra. The **LDOS** on site i is given by

$$\tilde{\rho}_i(\omega) := -\frac{1}{\pi} \text{Im} \mathcal{G}_{ii}^{R,\sigma}(\omega), \quad (54)$$

and is attainable via the diagonal components of $\mathcal{G}^{R,\sigma}(\omega)$. This is the Fourier transform ¹ of the dynamical correlation function in time (or many-body Green's function) $G^{R,\sigma}(t)$ defined as

$$G_{ii}^{R,\sigma}(t) := -i\theta(t)\langle\{c_{i,\sigma}^\dagger(t), c_{i,\sigma}\}\rangle_0 \quad (55)$$

where the overlap $\langle \rangle_0$ is taken over the ground state. $\theta(t)$ is the Heaviside step function to impose causality. There is a global spin symmetry under exchanging \uparrow and \downarrow such that $G_{ii}^{R,\uparrow}(t) = G_{ii}^{R,\downarrow}(t)$. We therefore restrict ourselves to considering just the spin up sector and drop the spin index. Since the dimer is invariant under swapping of sites, the two sites have equivalent **LDOS** and we fix $i = 1$. For the spinful interacting Fermi-Hubbard dimer without any dephasing, the zero-temperature equilibrium Greens function has an analytical solution in the Lehmann representation [86], whose poles can be obtained exactly. These correspond to the energies required for adding/removing an electron and are used as reference points in [Fig. 6](#). The effect of dissipation captured by the evolution with Lindbladians [Eq. \(53\)](#) and [Eq. \(25\)](#) on the **LDOS** of the dimer is shown in [Figure 6](#). The **LDOS** spectrum is symmetric under $\omega \rightarrow -\omega + c$ for constant c due to particle-hole symmetry. The time truncation window and number of samples affect the **FFT** to give the non uniform intensity profile shown in the first row of [Fig. 6](#). For the second and third row, the dimer evolves subject to the Lindbladians [Eq. \(53\)](#) and [Eq. \(25\)](#) respectively. In the second row, the 'stochastic' simulation method corresponds to [Theorem 1](#), i.e. the expectation over stochastic channels. This is much cheaper than full statevector simulation as it reduces the Hilbert space from dimension D to \sqrt{D} . The effect of dephasing on the time signal is an exponential dampening factor, and hence manifests in the **FFT** as a Lorentzian envelope around the underlying frequencies. This is clearly demonstrated in [Fig. 6](#), whereby an increase in g increases the Lorentzian width. This smearing effect also uniformises the peak intensities by softening the abrupt time truncation window. The main difference in the two dephasing Lindbladians on the dimer **LDOS** under the same coupling strength g is the resulting Lorentzian width. In the third row, the exact Lindbladian simulation is again not included. A quantifiable error bound does not exist for this simulation due to the truncation of the bosonic Hilbert space. On the other hand, Dcube computes $G_{ii}^{R,\sigma}(t)$ in the infinite boson Hilbert space *and* has the promise of being theoretically bounded by Trotter error. We provide a comparative study of 'exact Lindbladian' vs Dcube simulation for $G_{ii}^{R,\sigma}(t)$ in [Section C](#) at short times, where for sufficiently large number of Trotter steps, the main error is due to the bosonic truncation. This is similar to what has been done for fermion densities in [Fig. 3](#) and [Fig. 4](#).

¹ Formally, the Fourier transform is defined as

$$\tilde{G}^{R,\sigma}(\omega) := \int_{-\infty}^{\infty} G^{R,\sigma}(t) e^{-i\omega t} dt$$

where the integral extends to infinity. Practically, we compute the dynamical correlation function $G_{ii}^{R,\sigma}(t)$ as a time truncated signal with some fixed sampling rate. Therefore, $\mathcal{G}_{ii}^{R,\sigma}(\omega)$ as defined in the text is an approximation of $\tilde{G}^{R,\sigma}(\omega)$. Thus, if $G_{ii}^{R,\sigma}(t)$ is represented by a time signal x_1, \dots, x_M with M points, then $\mathcal{G}_{ii}^{R,\sigma}(\omega)$ is computed through the **Fast Fourier Transform (FFT)**

$$\mathcal{G}_{ii}^{R,\sigma}(\omega) := \sum_{p=1}^{p=M} x_p e^{-\frac{i2\pi\omega p}{M}}$$

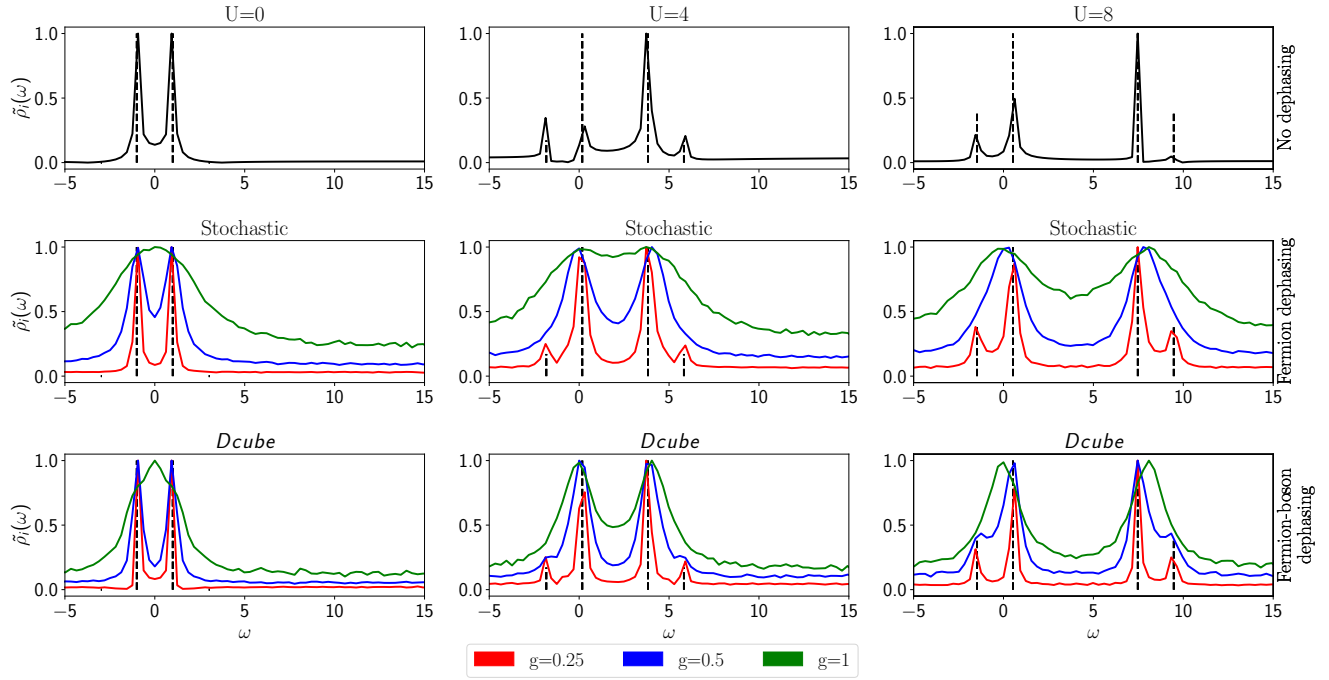


Figure 6. LDOS of the spinful Fermi-Hubbard dimer under two different types of dephasing at half-filling with $S_z = 0$ at site $i = 1$. Each column denotes a fixed interaction strength U . The vertical dashed lines denote the analytical peaks of the one-body Green's function for the dimer with no dephasing. Along row one, the solid black lines denote the rescaled imaginary component of the FFT of the truncated time signal $G_{11}(t)$. Along the second and third row, the dimer is subject to the Lindbladians Eq. (53) and Eq. (25) respectively. Different dephasing strengths g are denoted by different colours. The method for computing the second row named ‘stochastic’ is by producing the expectation value from 30k stochastic channels through the application of Theorem 1 with $N = 15$ first order Trotter steps. Dcube is used as the simulation method on the third row, with $N = 10$ first order Trotter steps, 10k IQP samples, $N_\eta = 10$ and $N_\rho = 2$ second order ($p = 2$) Trotter steps to produce the map G in Eq. (42). The total time evolution for all signals were performed up to $T = 20$ with 100 time point samples.

V. CONCLUSION

The simulation of open quantum systems is fundamental to many aspects of physics, such as material science and condensed matter physics. Accurate simulations of open systems can quickly become intractable upon considering relevant environmental effects [87]. In this work we develop quantum algorithms capable of simulating Lindbladian dynamics (arguably the simplest type of evolution characterising open quantum systems). We highlight two main contributions of this work, the first is a framework for simulating general Lindbladians via sampling unitary channels. We provide an explicit algorithm to simulate unital Lindbladians without requiring additional qubits and a generalisation to simulate general Lindbladians using with and additional ancillary qubits; the second introduces a decoupling scheme that reduces the complexity of Lindbladians consisting of interacting subsystems.

This decoupling scheme is particularly helpful when discussing systems coupled to bosonic degrees of freedom. Bosons have an infinite dimensional Hilbert space and then any finite dimensional representation introduces an error. Although in systems where the energy is conserved this error can be upper bounded [88–90], estimating this error in practice may be difficult. Using the decoupling algorithm we find that the evolution of bosons coupled to fermions can be approximated by sampling an IQP circuit, and using the sampled bitstring to define a fermionic circuit. This realises a unital channel on the fermions with a time dependent probability distribution, thus going beyond the Markovian approximation.

We perform numerical simulations of a fermion-boson coupled system undergoing dephasing, which in itself consists of both fermionic and bosonic components. This illustrative example focuses on fermion dynamics, and brings attention to multiple issues surrounding the exact Lindbladian simulation involving bosons. One notable problem that we highlight is the issue of truncation of the bosonic Hilbert space. Although the simulation for a fixed truncation can appear to be converged and well behaved, increasing the truncation level can still affect the dynamics, signaling the error introduced by introducing an arbitrary cut-off.

The decoupling framework presented here is an accessible way of studying non-Markovian dynamics on a quantum

computer and we envision several applications and generalisations to other practical scenarios. The connection with sampling IQP circuits suggests that simulating unital Lindbladians including bosons could be classically difficult in general, even though the infinite temperature state is a fixed point of the dynamics.

VI. ACKNOWLEDGMENTS

We would like to thank Ashley Montanaro, Raul Garcia-Patron and Jan Lukas Bosse for helpful discussions relating to IQP circuits, as well as algorithmic details and applications.

[1] D. W. Berry, G. Ahokas, R. Cleve, and B. C. Sanders, Efficient quantum algorithms for simulating sparse Hamiltonians, *Commun. Math. Phys.* **270**, 359 (2006).

[2] A. M. Childs and R. Kothari, Limitations on the simulation of non-sparse Hamiltonians, *Quantum Inf. Comput.* **10**, 669 (2010).

[3] D. W. Berry, A. M. Childs, R. Cleve, R. Kothari, and R. D. Somma, Exponential improvement in precision for simulating sparse Hamiltonians, in *Proceedings of the forty-sixth annual ACM symposium on Theory of computing* (ACM, 2014).

[4] D. W. Berry, A. M. Childs, R. Cleve, R. Kothari, and R. D. Somma, Simulating hamiltonian dynamics with a truncated taylor series, *Physical Review Letters* **114**, 10.1103/physrevlett.114.090502 (2015).

[5] G. H. Low and I. L. Chuang, Optimal Hamiltonian simulation by quantum signal processing, *Phys. Rev. Lett.* **118**, 010501 (2017).

[6] G. H. Low and I. L. Chuang, Hamiltonian simulation by qubitization, *Quantum* **3**, 163 (2019).

[7] A. M. Childs, Y. Su, M. C. Tran, N. Wiebe, and S. Zhu, Theory of Trotter error with commutator scaling, *Phys. Rev. X* **11**, 011020 (2021).

[8] D. Deutsch, Quantum theory, the church–turing principle and the universal quantum computer, *Proceedings of the Royal Society of London. A. Mathematical and Physical Sciences* **400**, 97 (1985).

[9] S. Somaroo, C. H. Tseng, T. F. Havel, R. Laflamme, and D. G. Cory, Quantum simulations on a quantum computer, *Physical Review Letters* **82**, 5381–5384 (1999).

[10] A. Miessen, P. J. Ollitrault, F. Tacchino, and I. Tavernelli, Quantum algorithms for quantum dynamics, *Nature Computational Science* **3**, 25 (2023).

[11] F. Alam, J. L. Bosse, I. Čepaitė, A. Chapman, L. Clinton, M. Crichigno, E. Crosson, T. Cubitt, C. Derby, O. Dowinton, P. K. Faehrmann, S. Flammia, B. Flynn, F. M. Gambetta, R. García-Patrón, M. Hunter-Gordon, G. Jones, A. Khedkar, J. Klassen, M. Kreshchuk, E. H. McMullan, L. Mineh, A. Montanaro, C. Mora, J. J. L. Morton, D. Patel, P. Rolph, R. A. Santos, J. R. Seddon, E. Sheridan, W. Somogyi, M. Svensson, N. Vaishnav, S. Y. Wang, and G. Wright, *Fermionic dynamics on a trapped-ion quantum computer beyond exact classical simulation* (2025), arXiv:2510.26300 [quant-ph].

[12] F. Alam, J. L. Bosse, I. Čepaitė, A. Chapman, L. Clinton, M. Crichigno, E. Crosson, T. Cubitt, C. Derby, O. Dowinton, P. K. Faehrmann, S. Flammia, B. Flynn, F. M. Gambetta, R. García-Patrón, M. Hunter-Gordon, G. Jones, A. Khedkar, J. Klassen, M. Kreshchuk, E. H. McMullan, L. Mineh, A. Montanaro, C. Mora, J. J. L. Morton, D. Patel, P. Rolph, R. A. Santos, J. R. Seddon, E. Sheridan, W. Somogyi, M. Svensson, N. Vaishnav, S. Y. Wang, and G. Wright, *Programmable digital quantum simulation of 2d fermi-hubbard dynamics using 72 superconducting qubits* (2025), arXiv:2510.26845 [quant-ph].

[13] E. Granet, S.-H. Lin, K. Hémery, R. Hagshenas, P. Andres-Martinez, D. T. Stephen, A. Ransford, J. Arkinstall, M. S. Allman, P. Campora, S. F. Cooper, R. D. Delaney, J. M. Dreiling, B. Estey, C. Figgatt, C. Foltz, J. P. Gaebler, A. Hall, A. Husain, A. Isanaka, C. J. Kennedy, N. Kotibhaskar, M. Mills, A. R. Milne, A. J. Park, A. P. Reed, B. Neyenhuis, J. G. Bohnet, M. Foss-Feig, A. C. Potter, R. Nigmatullin, M. Iqbal, and H. Dreyer, *Superconducting pairing correlations on a trapped-ion quantum computer* (2025), arXiv:2511.02125 [quant-ph].

[14] X. Li and C. Wang, Succinct description and efficient simulation of non-markovian open quantum systems, *Communications in Mathematical Physics* **401**, 147–183 (2023).

[15] V. Gorini, A. Kossakowski, and E. C. G. Sudarshan, Completely Positive Dynamical Semigroups of N Level Systems, *J. Math. Phys.* **17**, 821 (1976).

[16] G. Lindblad, On the generators of quantum dynamical semigroups, *Communications in Mathematical Physics* **48**, 119 (1976).

[17] H.-P. Breuer and F. Petruccione, *The Theory of Open Quantum Systems* (Oxford University Press, 2007).

[18] F. Verstraete, M. M. Wolf, and J. I. Cirac, Quantum computation and quantum-state engineering driven by dissipation, *Nature Physics* **5**, 633 (2009).

[19] M. Kliesch, T. Barthel, C. Gogolin, M. Kastoryano, and J. Eisert, Dissipative quantum church-turing theorem, *Physical Review Letters* **107**, 10.1103/physrevlett.107.120501 (2011).

[20] A. M. Childs and T. Li, Efficient simulation of sparse Markovian quantum dynamics, *Quant. Inf. Comput.* **17**, 0901 (2017), arXiv:1611.05543 [quant-ph].

[21] R. Cleve and C. Wang, Efficient quantum algorithms for simulating lindblad evolution (2019), arXiv:1612.09512 [quant-ph].

[22] A. W. Schlimgen, K. Head-Marsden, L. M. Sager, P. Narang, and D. A. Mazziotti, Quantum simulation of open quantum systems using a unitary decomposition of operators, *Phys. Rev. Lett.* **127**, 270503 (2021).

[23] A. W. Schlimgen, K. Head-Marsden, L. M. Sager, P. Narang, and D. A. Mazziotti, Quantum simulation of the lindblad equation using a unitary decomposition of operators, *Phys. Rev. Res.* **4**, 023216 (2022).

[24] J. Joo and T. P. Spiller, Commutation simulator for open quantum dynamics, *New Journal of Physics* **25**, 083041 (2023).

[25] X. Li and C. Wang, *Simulating markovian open quantum systems using higher-order series expansion* (2023), [arXiv:2212.02051 \[quant-ph\]](https://arxiv.org/abs/2212.02051).

[26] N. Suri, J. Barreto, S. Hadfield, N. Wiebe, F. Wudarski, and J. Marshall, Two-Unitary Decomposition Algorithm and Open Quantum System Simulation, *Quantum* **7**, 1002 (2023).

[27] T. Watad and N. H. Lindner, *Variational quantum algorithms for simulation of lindblad dynamics* (2023), [arXiv:2305.02815 \[quant-ph\]](https://arxiv.org/abs/2305.02815).

[28] G. Di Bartolomeo, M. Vischi, T. Feri, A. Bassi, and S. Donadi, Efficient quantum algorithm to simulate open systems through a single environmental qubit, *Physical Review Research* **6**, [10.1103/physrevresearch.6.043321](https://doi.org/10.1103/physrevresearch.6.043321) (2024).

[29] E. Borras and M. Marvian, Quantum algorithm to simulate lindblad master equations, *Phys. Rev. Res.* **7**, 023076 (2025).

[30] Z. Ding, X. Li, and L. Lin, Simulating open quantum systems using hamiltonian simulations, *PRX Quantum* **5**, 020332 (2024).

[31] M. Pocnic, D. Segal, and N. Wiebe, *Quantum simulation of lindbladian dynamics via repeated interactions* (2025), [arXiv:2312.05371 \[quant-ph\]](https://arxiv.org/abs/2312.05371).

[32] A. M. Childs, D. Maslov, Y. Nam, N. J. Ross, and Y. Su, Toward the first quantum simulation with quantum speedup, *Proc. Natl. Acad. Sci. U.S.A.* **115**, 9456 (2018).

[33] A. M. Childs and Y. Su, Nearly optimal lattice simulation by product formulas, *Phys. Rev. Lett.* **123**, 050503 (2019).

[34] J. L. Bosse, A. M. Childs, C. Derby, F. M. Gambetta, A. Montanaro, and R. A. Santos, Efficient and practical hamiltonian simulation from time-dependent product formulas, *Nature Communications* **16**, [10.1038/s41467-025-57580-5](https://doi.org/10.1038/s41467-025-57580-5) (2025).

[35] K. M. R. Audenaert and S. Scheel, On random unitary channels, *New Journal of Physics* **10**, 023011 (2008).

[36] M. V. Medvedyeva, F. H. Essler, and T. Prosen, Exact bethe ansatz spectrum of a tight-binding chain with dephasing noise, *Physical Review Letters* **117**, [10.1103/physrevlett.117.137202](https://doi.org/10.1103/physrevlett.117.137202) (2016).

[37] S. Longhi, Anderson localization in dissipative lattices, *Annalen der Physik* **535**, [10.1002/andp.202200658](https://doi.org/10.1002/andp.202200658) (2023).

[38] M. Žnidarič, Dephasing-induced diffusive transport in the anisotropic heisenberg model, *New Journal of Physics* **12**, 043001 (2010).

[39] M. H. Fischer, M. Maksymenko, and E. Altman, Dynamics of a many-body-localized system coupled to a bath, *Physical Review Letters* **116**, [10.1103/physrevlett.116.160401](https://doi.org/10.1103/physrevlett.116.160401) (2016).

[40] M. V. Medvedyeva, T. c. v. Prosen, and M. Žnidarič, Influence of dephasing on many-body localization, *Phys. Rev. B* **93**, 094205 (2016).

[41] E. Levi, M. Heyl, I. Lesanovsky, and J. P. Garrahan, Robustness of many-body localization in the presence of dissipation, *Physical Review Letters* **116**, [10.1103/physrevlett.116.237203](https://doi.org/10.1103/physrevlett.116.237203) (2016).

[42] S. Marcantoni, F. Carollo, F. M. Gambetta, I. Lesanovsky, U. Schneider, and J. P. Garrahan, Anderson and many-body localization in the presence of spatially correlated classical noise, *Physical Review B* **106**, [10.1103/physrevb.106.134211](https://doi.org/10.1103/physrevb.106.134211) (2022).

[43] P. Rebentrost, M. Mohseni, I. Kassal, S. Lloyd, and A. Aspuru-Guzik, Environment-assisted quantum transport, *New Journal of Physics* **11**, 033003 (2009).

[44] X. Turkeshi and M. Schiró, Diffusion and thermalization in a boundary-driven dephasing model, *Phys. Rev. B* **104**, 144301 (2021).

[45] S. Longhi, Dephasing-induced mobility edges in quasicrystals, *Phys. Rev. Lett.* **132**, 236301 (2024).

[46] T. G. Kiely and C. Xu, *Phase transition of topological index driven by dephasing* (2025), [arXiv:2506.04102 \[cond-mat.str-el\]](https://arxiv.org/abs/2506.04102).

[47] D. Lonigro and D. Chruściński, On the classicality of quantum dephasing processes, *Frontiers in Quantum Science and Technology Volume 1 - 2022*, [10.3389/frqst.2022.1090022](https://doi.org/10.3389/frqst.2022.1090022) (2022).

[48] M. J. Bremner, R. Jozsa, and D. J. Shepherd, Classical simulation of commuting quantum computations implies collapse of the polynomial hierarchy, *Proceedings of the Royal Society A: Mathematical, Physical and Engineering Sciences* **467**, 459–472 (2010).

[49] M. J. Bremner, A. Montanaro, and D. J. Shepherd, Average-case complexity versus approximate simulation of commuting quantum computations, *Physical Review Letters* **117**, [10.1103/physrevlett.117.080501](https://doi.org/10.1103/physrevlett.117.080501) (2016).

[50] A. Werner, D. Jascke, P. Silvi, M. Kliesch, T. Calarco, J. Eisert, and S. Montangero, Positive tensor network approach for simulating open quantum many-body systems, *Physical Review Letters* **116**, [10.1103/physrevlett.116.237201](https://doi.org/10.1103/physrevlett.116.237201) (2016).

[51] A. Sander, M. Fröhlich, M. Eigel, J. Eisert, P. Gelfß, M. Hintermüller, R. M. Milbradt, R. Wille, and C. B. Mendl, *Large-scale stochastic simulation of open quantum systems* (2025), [arXiv:2501.17913 \[quant-ph\]](https://arxiv.org/abs/2501.17913).

[52] T. Holstein, Studies of polaron motion: Part i. the molecular-crystal model, *Annals of physics* **8**, 325 (1959).

[53] H. Fröhlich, Electrons in lattice fields, *Advances in Physics* **3**, 325 (1954).

[54] J. Tempere, W. Casteels, M. Oberthaler, S. Knoop, E. Timmermans, and J. Devreese, Feynman path-integral treatment of the bec-impurity polaron, *Physical Review B* **80**, 184504 (2009).

[55] J. Bardeen, L. N. Cooper, and J. R. Schrieffer, Theory of superconductivity, *Physical review* **108**, 1175 (1957).

[56] C. Kvande, C. Feng, F. Hébert, G. Batrouni, and R. Scalettar, Enhancement of charge density wave correlations in a holstein model with an anharmonic phonon potential, *Physical Review B* **108**, 075119 (2023).

[57] R. P. Feynman, Slow electrons in a polar crystal, *Physical Review* **97**, 660 (1955).

[58] N. Prokof'ev and B. Svistunov, Bold diagrammatic monte carlo: A generic sign-problem tolerant technique for polaron models and possibly interacting many-body problems, *Physical Review B* **77**, 125101 (2008).

[59] A. S. Mishchenko, N. Nagaosa, and N. Prokof'ev, Diagrammatic monte carlo method for many-polaron problems, *Physical Review Letters* **113**, 166402 (2014).

[60] T. Hahn, S. Klimin, J. Tempere, J. T. Devreese, and C. Franchini, Diagrammatic monte carlo study of fröhlich polaron dispersion in two and three dimensions, *Physical Review B* **97**, 134305 (2018).

[61] D. Sels, Dynamic polaron response from variational imaginary time evolution, arXiv preprint arXiv:1605.04998 [10.48550/arXiv.1605.04998](https://arxiv.org/abs/1605.04998) (2016).

[62] J. Vlietinck, W. Casteels, K. Van Houcke, J. Tempere, J. Ryckebusch, and J. T. Devreese, Diagrammatic monte carlo study of the acoustic and the bose-einstein condensate polaron, *New Journal of Physics* **17**, 033023 (2015).

[63] A. Taheridehkordi, S. Curnoe, and J. LeBlanc, Algorithmic matsubara integration for hubbard-like models, *Physical Review B* **99**, 035120 (2019).

[64] J. Vučičević and M. Ferrero, Real-frequency diagrammatic monte carlo at finite temperature, *Physical Review B* **101**, 075113 (2020).

[65] M. Houtout, L. Ranalli, C. Verdi, S. Klimin, S. Ragni, C. Franchini, and J. Tempere, Anharmonic long-range electron-phonon interaction: analytic formalism, arXiv preprint arXiv:2412.09470 [10.48550/arXiv.2412.09470](https://arxiv.org/abs/2412.09470) (2024).

[66] W. Cochran, Crystal stability and the theory of ferroelectricity, *Advances in Physics* **9**, 387 (1960).

[67] T. A. Mellan, A. Aziz, Y. Xia, R. Grau-Crespo, and A. I. Duff, Electron and phonon interactions and transport in the ultrahigh-temperature ceramic zrc, *Physical Review B* **99**, 094310 (2019).

[68] D. Hooton, Li. a new treatment of anharmonicity in lattice thermodynamics: I, *The London, Edinburgh, and Dublin Philosophical Magazine and Journal of Science* **46**, 422 (1955).

[69] N. Werthamer, Self-consistent phonon formulation of anharmonic lattice dynamics, *Physical Review B* **1**, 572 (1970).

[70] M. Zacharias, G. Volonakis, F. Giustino, and J. Even, Anharmonic lattice dynamics via the special displacement method, *Physical Review B* **108**, 035155 (2023).

[71] A. F. White, Y. Gao, A. J. Minnich, and G. K. Chan, A coupled cluster framework for electrons and phonons, *The Journal of Chemical Physics* **153**, 10.1063/5.0033132 (2020).

[72] G. Paleari, F. Hébert, B. Cohen-Stead, K. Barros, R. T. Scalettar, and G. G. Batrouni, Quantum monte carlo study of an anharmonic holstein model, *Physical Review B* **103**, 195117 (2021).

[73] P. E. Dolgirev, J. Marino, D. Sels, and E. Demler, Non-gaussian correlations imprinted by local dephasing in fermionic wires, *Physical Review B* **102**, 100301 (2020).

[74] Y.-W. Huang and W.-M. Zhang, Exact master equation for generalized quantum brownian motion with momentum-dependent system-environment couplings, *Physical Review Research* **4**, 033151 (2022).

[75] A. G. Redfield, On the theory of relaxation processes, *IBM Journal of Research and Development* **1**, 19 (1957).

[76] E. B. Davies, Markovian master equations, *Communications in mathematical Physics* **39**, 91 (1974).

[77] R. K. Wangsness and F. Bloch, The dynamical theory of nuclear induction, *Physical Review* **89**, 728 (1953).

[78] A. Lampo, S. H. Lim, J. Wehr, P. Massignan, and M. Lewenstein, Lindblad model of quantum brownian motion, *Physical Review A* **94**, 042123 (2016).

[79] B. M. Terhal and D. P. DiVincenzo, Classical simulation of noninteracting-fermion quantum circuits, *Physical Review A* **65**, 032325 (2002).

[80] M. J. Bremner, A. Montanaro, and D. J. Shepherd, Average-case complexity versus approximate simulation of commuting quantum computations, arXiv preprint arXiv:1504.07999 (2015).

[81] M. J. Bremner, R. Jozsa, and D. J. Shepherd, Classical simulation of commuting quantum computations implies collapse of the polynomial hierarchy, *Proceedings of the Royal Society A: Mathematical, Physical and Engineering Sciences* **467**, 459 (2011).

[82] S. Aaronson and A. Arkhipov, The computational complexity of linear optics, in *Proceedings of the forty-third annual ACM symposium on Theory of computing* (2011) pp. 333–342.

[83] A. Picano, M. Vanhoecque, and M. Schirò, Heating dynamics of correlated fermions under dephasing, arXiv preprint arXiv:2507.21804 (2025).

[84] V. Alba, *Free fermions with dephasing and boundary driving: Bethe ansatz results*, scipost phys (2025).

[85] E. N. Economou, *Green's functions in quantum physics* (Springer, 2006).

[86] P. Romaniello, Hubbard dimer in gw and beyond, *Lecture Notes of the Autumn School on Correlated Electrons 2021–Simulating Correlations with Computers* (2021).

[87] I. Luchnikov, S. Vintskevich, H. Ouerdane, and S. Filippov, Simulation complexity of open quantum dynamics: Connection with tensor networks, *Physical review letters* **122**, 160401 (2019).

[88] M. P. Woods, M. Cramer, and M. B. Plenio, Simulating bosonic baths with error bars, *Physical Review Letters* **115**, 130401 (2015).

[89] Y. Tong, V. V. Albert, J. R. McClean, J. Preskill, and Y. Su, Provably accurate simulation of gauge theories and bosonic systems, *Quantum* **6**, 816 (2022).

[90] F. Arzani, R. I. Booth, and U. Chabaud, Effective descriptions of bosonic systems can be considered complete, *Nature Communications* **16**, 9744 (2025).

[91] M. Born, Quantenmechanik der stoßvorgänge, *Zeitschrift für physik* **38**, 803 (1926).

Appendix A: Proof of Theorem 1

The aim of this section is to bound the distance between the mixed unitary channel $\mathcal{E}(\rho) = \sum_{\mathbf{s}=\{+,-\}^N} p_{\mathbf{s}} \mathcal{U}_{\mathbf{s}}(\rho)$, with $\mathcal{U}_{\mathbf{s}}$ defined in Eq. (5) and the evolution generated by \mathcal{L} . For simplicity we will be setting the coherent part to zero ($H = 0$) here as this is just captured by the usual first order Trotter error)

To this end we define two auxiliary channels

$$\Omega_{k,t}() := \sum_{\mathbf{s}=\{+,-\}^j} \frac{1}{2^k} \prod_{j=1}^k e^{is_j \sqrt{t} L_j}() e^{-is_j \sqrt{t} L_j} = \prod_j \omega_{j,t}() \quad (\text{A1})$$

and $e^{it\mathcal{L}_j}$, where $\mathcal{L}_j(\rho) = \sum_{i=1}^j L_i(\rho) L_i - \frac{1}{2} \{L_i^2, \rho\}$. Using these channels and the properties of the telescopic sum with $\mathcal{L}_0 = 0$ and $\Omega_{0,t} = 1$ we have

$$\|\Omega_{N,t} - e^{t\mathcal{L}_N}\|_{\diamond} = \left\| \sum_{j=1}^N \Omega_{j,t} e^{t(\mathcal{L}_N - \mathcal{L}_j)} - \Omega_{j-1,t} e^{t(\mathcal{L}_N - \mathcal{L}_{j-1})} \right\|_{\diamond} \quad (\text{A2})$$

$$\leq \sum_{j=1}^N \left\| \Omega_{j-1,t} (\omega_{j,t} - e^{t(\mathcal{L}_N - \mathcal{L}_{j-1})} e^{-t(\mathcal{L}_N - \mathcal{L}_j)}) e^{t(\mathcal{L}_N - \mathcal{L}_j)} \right\|_{\diamond} \quad (\text{A3})$$

where the first equality is an identity of telescopic sums and the last inequality is a consequence of the triangle inequality. Using the submultiplicative property of the diamond norm and the fact that the diamond norm of a CPTP map is equal to one, the last inequality becomes

$$\|\Omega_{N,t} - e^{t\mathcal{L}_N}\|_{\diamond} \leq \sum_{j=1}^N \left\| \omega_{j,t} - e^{t(\mathcal{L}_N - \mathcal{L}_{j-1})} e^{-t(\mathcal{L}_N - \mathcal{L}_j)} \right\|_{\diamond} \quad (\text{A4})$$

$$\leq \sum_{j=1}^N \left\| \omega_{j,t} - e^{t(\mathcal{L}_j - \mathcal{L}_{j-1})} \right\|_{\diamond} + \sum_{j=1}^N \left\| e^{t(\mathcal{L}_j - \mathcal{L}_{j-1})} - e^{t(\mathcal{L}_N - \mathcal{L}_{j-1})} e^{-t(\mathcal{L}_N - \mathcal{L}_j)} \right\|_{\diamond} \quad (\text{A5})$$

where $\text{Adj}_A := [A, \cdot]$ and $\text{Adj}_A^n() = [\text{Adj}_A^{n-1}(), ()]$ the last inequality follows from the triangle inequality. The last term above is $O(t^2)$ by usual Trotter bounds, so we concentrate on the first one.

Let's define $\ell_j() = \mathcal{L}_j() - \mathcal{L}_{j-1}()$ and

$$E_{j,t} := \omega_{j,t} - e^{t(\mathcal{L}_j - \mathcal{L}_{j-1})} = \sum_{m=0}^{\infty} t^m \left(\frac{(-1)^m}{(2m)!} \text{Adj}_{L_j}^{2m}() - \frac{\ell_j^m()}{m!} \right) \quad (\text{A6})$$

now using that $\text{Adj}_{L_j}^0() = 1$ and

$$\text{Adj}_{L_j}^2() = [L_j, [L_j, ()]] = [L_j, L_j() - ()L_j] = \{L_j^2, ()\} - 2L_j()L_j = -\ell_j \quad (\text{A7})$$

by induction it follows that $\text{Adj}_{L_j}^{2m} = (-1)^m \ell_j^m$, so we have

$$E_{j,t} = \sum_{m=2}^{\infty} t^m \left(\frac{1}{(2m)!} - \frac{1}{m!} \right) \ell_j^m \quad (\text{A8})$$

finally, for $t \in [0, 1]$, $t^2 \geq t^m$ so

$$\|E_{j,t}\|_{\diamond} \leq t^2 \sum_{m=2}^{\infty} \left| \frac{1}{(2m)!} - \frac{1}{m!} \right| \|\ell_j^m\|_{\diamond} \quad (\text{A9})$$

which proves Theorem 1.

Appendix B: Electron phonon interacting Lindbladian derivation

Here we discuss the origins of the electron-phonon Lindbladian Eq. (25) from the main text. We start from a closed system of L sites whose Hamiltonian consists of fermions and bosons given by Eq. (B1). For concreteness, we write for the fermion subsystem H_F , a quartic Hamiltonian with creation (annihilation) operators denoted by c^\dagger (c). This choice of H_F can be arbitrary as it eventually will only play a role in the unitary evolution. The boson subsystem is further divided into Brownian and bath particles residing on each site i , whose creation (annihilation) operators are denoted by $q^\dagger(q)$ and $b^\dagger(b)$ respectively.

$$H_T = \left[\sum_{ijkl} c_i^\dagger c_j + h.c. + V_{ijkl} c_i^\dagger c_j^\dagger c_c c_k \right] (H_F) + \left[\sum_i \omega_i q_i^\dagger q_i \right] \text{Brownian particle } (H_Q) + \left[\sum_i \frac{g_i}{\sqrt{2\pi}} x_i X_{i,\alpha} \left(c_i^\dagger c_i - \frac{1}{2} \right) \right] \text{2nd order int } (H_{FQB}) + \left[\sum_{i,\alpha} \tilde{\omega}_{i,\alpha} b_{i,\alpha}^\dagger b_{i,\alpha} \right] \text{Bath } (H_B) \quad (\text{B1})$$

The fermions and bosons on site i are coupled to each other with strength $\frac{g_i}{\sqrt{2\pi}}$, and $\tilde{\omega}_{i,\alpha}$ (ω_i) denote the bath (Brownian particle) harmonic oscillator frequencies respectively. α is a frequency index. $x_i := \frac{q_i^\dagger + q_i}{\sqrt{2}}$ and $X_{i,\alpha} := \frac{b_{i,\alpha}^\dagger + b_{i,\alpha}}{\sqrt{2}}$ denote the position operators for the Brownian and bath particles respectively. From here on we work in the interaction picture of the bath, H_B . For simplicity, we renormalise such that $\hbar = 1$ and assume that each site has the same coupling strength $\frac{g_i}{\sqrt{2\pi}} = \frac{g}{\sqrt{2\pi}}$, $\forall i$. The total Hamiltonian in the interaction picture is therefore

$$H_I(t) = H_F + H_Q + e^{-itH_B} H_{FQB} e^{itH_B} \quad (\text{B2})$$

$$= H_F + H_Q + H_{FQB}(t). \quad (\text{B3})$$

Using the boson commutation relations, the interaction Hamiltonian between different subsystems simplifies to

$$H_{FQB}(t) = \sum_{i,\alpha} \frac{g}{\sqrt{2\pi}} x_i \left(c_i^\dagger c_i - \frac{1}{2} \right) X_{i,\alpha}(t) \quad (\text{B4})$$

where $X_{i,\alpha}(t) = e^{-itH_B} X_{i,\alpha} e^{itH_B}$. Under the Born approximation [91] (i.e. weak coupling with bath) we approximate the total density matrix as $\rho_T(t) \approx \rho_{FQ}(t) \otimes \rho_B$. Assuming that the bath is memoryless, we apply the Markov assumption [75, 76] and the BMME is given by

$$\frac{d}{dt} \rho_{FQ}(t) = -i \text{tr}_B([H_I(t), \rho_{FQ}(t) \otimes \rho_B]) - \int_0^\infty ds \text{tr}_B([H_I(t), [H_I(t-s), \rho_{FQ}(t) \otimes \rho_B]]) \quad (\text{B5})$$

We will refer to the first and second term of Eq. (B5) as the unitary \mathcal{L}_U and dissipative \mathcal{L}_D components. Consider the case where the bath is initially in the vacuum state such that

$$\text{Tr}_B(\rho_B X_{i,\alpha}) = 0, \forall i, \alpha \quad (\text{B6})$$

Using Eq. (B6), the unitary evolution component of the BMME in Eq. (B5) therefore simplifies to

$$\mathcal{L}_U(\rho_{FQ}(t)) = -i([H_F + H_Q, \rho_{FQ}(t)]) \quad (\text{B7})$$

after tracing out the bath, where the $H_{FQB}(t)$ term vanish. For the dissipative component \mathcal{L}_D , four of the commutator terms involving a single $H_{FQB}(t)$ are again zero using Eq. (B6). If we integrate Eq. (B5) with respect to time t , at short times the \mathcal{L}_U scales $O(t)$ and \mathcal{L}_D scales as $O(t^2)$. The four terms that are time-independent coming from $\text{tr}_B([H_F + H_Q, [H_F + H_Q, \rho_{FQ}(t) \otimes \rho_B]])$ scale as second order in time, i.e. $O(t^2)$ and are ignored. Thus, there is only one non-trivial term out of the nine to consider, given by

$$\mathcal{L}_D(\rho_{FQ}(t)) = - \int_0^\infty ds \text{tr}_B([H_{FQB}(t), [H_{FQB}(t-s), \rho_{FQ}(t) \otimes \rho_B]]) \quad (\text{B8})$$

If we assume that the brownian boson is initialised in the vacuum state, we arrive at the simplified relations

$$\begin{aligned} \int ds \frac{g^2}{2\pi} \text{tr}_B \left(\sum_{ij} X_i(t) X_j(t-s) \rho_B \right) &= \int ds \frac{g^2}{2\pi} \text{tr}_B \left(\sum_{ij} X_i(t-s) \rho_B X_j(t) \right) = \sum_{i,\alpha} \frac{g^2}{2\pi} \left(\int_0^\infty e^{-i\tilde{\omega}_{i,\alpha}s} ds \right) \\ \int ds \frac{g^2}{2\pi} \text{tr}_B \left(\sum_{ij} \rho_B X_i(t-s) X_j(t) \right) &= \int ds \frac{g^2}{2\pi} \text{tr}_B \left(\sum_{ij} X_i(t) \rho_B X_j(t-s) \right) = \sum_{i,\alpha} \frac{g^2}{2\pi} \left(\int_0^\infty e^{i\tilde{\omega}_{i,\alpha}s} ds \right) \end{aligned} \quad (\text{B9})$$

We also extend the integral to $-\infty$ and take the limit of a continuum of bath modes such that $\sum_{\alpha} \rightarrow \int d\tilde{\omega}_{\alpha}$ such that

$$\int d\tilde{\omega}_i \int_{-\infty}^{\infty} ds e^{\pm i\tilde{\omega}_{i,\alpha} s} = 2\pi \int d\tilde{\omega}_i \delta(\tilde{\omega}_i) = 2\pi \quad (\text{B10})$$

then Eq. (B8) simplifies to

$$\begin{aligned} \frac{d}{dt} \rho_{FQ}(t)(t) &= -i[H_F + H_Q, \rho_{FQ}(t)] \\ &+ \sum_i g^2 \left(x_i (n_i \rho_{FQ}(t) n_i - \frac{1}{2} \{n_i, \rho_{FQ}(t)\}) x_i + \frac{1}{4} (x_i \rho_{FQ}(t) x_i - \frac{1}{2} \{x_i^2, \rho_{FQ}(t)\}) \right) \end{aligned} \quad (\text{B11})$$

which is exactly the form of the Lindbladian Eq. (25) studied in the main text.

Appendix C: Simulating dynamical correlation function time dynamics

In this section, we plot the TDS of the dynamical correlation function $\text{Re} \left(\langle \{c_1^\dagger c_1(t)\} \rangle_0 \right)$ using Dcube and ‘exact Lindbladian’ methods. As shown in Fig. 7, truncating the boson Hilbert space in ‘exact Lindbladian’ simulations has immediate consequences at short times. This behavior was different for fermion densities studied in Fig. 4, which were more stable at short times. This highlights an important practical point, in that it is necessary to do a boson truncation study for *every* observable of interest. On the other hand, the error of Dcube is independent of the truncation, and converges in this particular case at $N_t = 5$ first order Trotter steps.

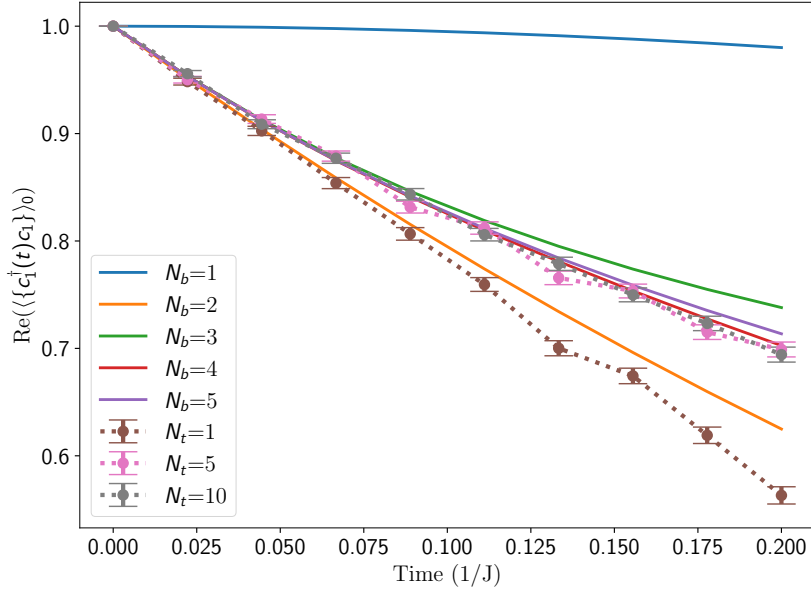


Figure 7. Time dynamics of $\text{Re} \left(\langle \{c_1^\dagger(t)c_1\} \rangle_0 \right)$ for the spinful dimer at half-filling at site one, $S_z = 0$ and $g = 1$. The solid lines denote exact Lindbladian statevector simulation with truncated Boson Hilbert space of with N_b levels (i.e. with maximum $N_b - 1$ bosons). The dashed lines denote using the Dcube algorithm (Theorem 4) with 10k IQP samples at various first order Trotter step sizes N_t . The error bars are taken as $\frac{\sigma}{\sqrt{N_s}}$ where σ is the sample standard deviation.